Received: 5 July 2022 | Revised: 11 October 2022 | Accepted: 11 November 2022

DOI: 10.1111/bre.12738

Basin Research | IAS EAGE | WILEY

RESEARCH ARTICLE

Relative sea-level control on the building of two distinct shelf-margin clinothems on the late-Quaternary Pearl River margin: Insights from numerical stratigraphic forward modelling

Kun Qi[1,2] | **Chenglin Gong**[1,2] | **Jinyu Zhang**[3] | **Katrine Juul Andresen**[4] | **Zhenkui Jin**[1,2]

[1]State Key Laboratory of Petroleum Resources and Prospecting, China University of Petroleum (Beijing), Beijing, China

[2]College of Geosciences, China University of Petroleum (Beijing), Beijing, China

[3]Bureau of Economic Geology, Jackson School of Geosciences, The University of Texas at Austin, Austin, Texas, USA

[4]Department of Geoscience, Aarhus University, Aarhus C, Denmark

Correspondence
Chenglin Gong, State Key Laboratory of Petroleum Resources and Prospecting, China University of Petroleum (Beijing), Beijing 102249, China.
Email: chenglingong@cup.edu.cn

Funding information
China University of Petroleum, Beijing, Grant/Award Number: 2462020YXZZ020; National Natural Science Foundation of China, Grant/Award Number: 41972100 and 41802117

Abstract

As one of the most important forcing factors, relative sea-level changes exert a major influence on the building of shelf-margin clinothems. However, it is still not well understood how these changes control the growth of shelf edges and the condition of sediments transporting into deep water, especially over the individual-clinothem scale of several 100 ky. On the late-Quaternary Pearl River margin, there are two distinct shelf-margin clinothems: SQ3 and SQ4. They have different shelf-edge trajectories (slight rising vs. steep rising) and different styles of deep-water deposition (fan lobes consisting mainly of MTDs vs. fan lobes consisting mainly of turbidites). This work takes those SQ3 and SQ4 as study objects and runs a total of 136 experiments from the Dionisos stratigraphic forward model to investigate how relative sea-level changes control the trajectories of shelf edges and the volumes of MTDs in deep water over the individual-clinothem scale. Our quantitative results suggest that under the geological background of high sediment supply on the late-Quaternary Pearl River margin, the duration of highstand systems tracts (HST) relative to lowstand systems tracts (LST) or forced regressive systems tracts (FST) has a significant influence on the building of individual shelf-margin clinothems. If the relative duration of HST is either very short or very long, slight-rising shelf-edge trajectories and large-volume MTDs would be formed, whereas if the relative duration of HST is comparable with LST or FST, steep-rising shelf-edge trajectories and limited MTDs would be formed. Through the constrains of the model set to the real geological condition of the SQ3 and SQ4 clinothems, it is found that SQ3 was caused by the quite long relative duration of HST, which made highstand deltaic systems advance over the pre-existing shelf-slope break, leading to significant accretion and instability of the shelf edge and thus, giving rise to the formation of slight-rising shelf-edge trajectories and fan lobes with high MTDs contents. SQ4, however, formed as a result of the comparable durations of HST, LST, and FST, which made highstand

deltaic systems advance to but not beyond the previous shelf-slope break allowing the subsequent FST to be directly perched on the clinoform slope. Such building processes did not drive pronounced accretion and instability of the shelf edge and thus, caused the formation of steep-rising shelf-edge trajectories and fan lobes with low MTDs contents.

KEYWORDS

late-Quaternary Pearl River margin, numerical stratigraphic forward modelling, relative sea-level changes, shelf-margin clinothems

1 | INTRODUCTION

Sediment supply to the continental shelf causes the building of shelf-margin sedimentary prisms, within which clinoforms are the time-line expressions of discrete phases of aggradation and accretion and clinothems are the equivalent rock units bounded by clinoforms (Posamentier & Allen, 1999; Posamentier et al., 1988; Pratson et al., 2004; Rich, 1951; Steel & Olsen, 2002). Those shelf-margin clinothems represent the basic regressive-to-transgressive building blocks in stratigraphic successions and reflect the style of continental margin building (Helland-Hansen et al., 2012; Helland-Hansen & Hampson, 2009; Johannessen & Steel, 2005). Therefore, it is a matter of significant scientific interest to understand their growth and associated controlling factors.

In general, shelf-margin clinothems grow in aggradational and progradational steps, during which shelf edges (areas of rollovers between the flat and the slope of clinoforms) migrate through time, forming a variety of shelf-edge trajectories and terrestrial sediments are transported into deep water, forming different characteristics of submarine deposits (Henriksen et al., 2009; Johannessen & Steel, 2005; Mellere et al., 2002; Olariu & Steel, 2009). Such building processes are potentially affected by multiple variables; apart from traditional sea-level controls, sediment supply (Carvajal et al., 2009), shelf width (Zhang et al., 2019), inherited topography (Prince & Burgess, 2013), and even autogenic process (Burgess et al., 2008) can all play a role. Nevertheless, relative sea-level changes are still considered to be the primary driving mechanism for the growth of shelf-margin clinothems, especially on those margins with shelf characteristics of great widths and gentle gradients (Catuneanu et al., 2009; Helland-Hansen & Hampson, 2009). The linkages among changes of relative sea level, growths of shelf edges, and the delivery of terrestrial sediments into the deep-water settings have been the subject of increasingly intense study in recent years (Gong, Qi, et al., 2019; Posamentier et al., 2019; Zhang et al., 2017). However, most of these works were conducted over a relatively large time scale (1 My or more), which only emphasized the long-term shelf-margin evolution; growth of individual clinothems, the basic building blocks of stratigraphic sequences, over relatively smaller time scales of several 100 ky is less studied (Catuneanu, 2019; Magyar et al., 2019). Due to the insufficient resolution of datasets and the problem in defining a previous relative sea-level cycle, relative sea-level modulations on the regressive-to-transgressive transits of deltaic systems, the geometry and internal architecture of clinothems, and the condition of sediments transporting into deep water are still not well understood. The method of numerical stratigraphic forward modelling, however, provides us an excellent opportunity to address those issues.

Highlights

- Building of the individual shelf-margin clinothems is quantitatively analyzed.
- Development of HST can significantly affect the building of shelf-margin clinothems.
- Differences between two clinothems on the late-Quaternary Pearl River margin are explained.

This paper takes two distinct shelf-margin clinothems on the late-Quaternary Pearl River margin as the study objects to explore their building along depositional dip as a function of relative sea-level changes. We follow the classic sequence stratigraphic conceptual models (two-dimensional conceptual models) and run a series of numerical simulations in a stratigraphic forward model called Dionisos, to examine the consequences of varying relative sea-level changes on the growth of shelf edges and the condition of sediments transporting into deep water over the individual-clinothem scale. Specifically, we first (1) briefly review our current understanding on the late-Quaternary Pearl River margin to estimate likely values of input parameters and setup a series of modelling experiments, then (2) analyse the growth style of shelf edges and the condition of sediment transporting into deep water for the individual clinothem generated in each model run to

establish linkages between clinothems and relative sea-level regimes, and finally (3) compare the two studied Pearl River shelf-margin clinothems with the modelled results to constrain their model counterparts and in turn, explain the well-observed differences between those two clinothmes based on internal stratigraphic processes.

2 | GEOLOGICAL SETTING AND PREVIOUS WORK

2.1 | Geological background of the late-Quaternary Pearl River margin

The study area is located in the central Pearl River Mouth Basin, which occupies an area of $1.75\times10^5\,km^2$ and belongs to the central part of the northern South China Sea margin (Figure 1a). The basin initiated as an elongated rift at 59 Ma, with two main stages of tectonic evolution, namely a Palaeocene to Oligocene synrift stage and a Miocene to Quaternary postrift stage (Franke et al., 2011; Ru & Pigott, 1986; Zhao et al., 2016). Since 23.8 Ma, that northern continental margin of the South China Sea has a prominent shelf-slope-basin physiography, into which the long-term active, Pearl River fluvial system debouched and formed widespread deltaic and deep-water deposits (Gong et al., 2013, 2018; Lin, He, et al., 2018; Lin, Jiang, et al., 2018; Zhuo et al., 2015). The present work focuses on the building of shelf-margin clinothems in the late Quaternary, that is, the fluvial-deltaic systems and coeval deep-water systems within the youngest and uppermost level of the stratigraphic succession in the central Pearl River Mouth Basin (Figure 1b,c). During the late Quaternary, the "Dongsha Tectonic Movement" was the most important neotectonic activity in the northern South China Sea (Li et al., 1999; Yao, 1999). It was caused by the convergence between the South China Sea and Philippine Sea plates and around the Dongsha Island: it is primarily expressed as the uplift of the Dongsha Rise, the formation of NWW-trending fault systems and large-scale thermal fluid movement (Yao & Yang, 2008; Zhao et al., 2012). In our study area to the west, the Dongsha Tectonic Movement, however, plays an important role on the subsidence and uplift of the continental margin (He et al., 2019; Lin, He, et al., 2018; Wang et al., 2020; Xie et al., 2017). Therefore, during the deposition of the late-Quaternary succession, the change of the relative sea level was significantly enhanced, with an amplitude up to 250 m (Lin, He, et al., 2018; Liu et al., 2019; Ludmann et al., 2001).

Based on the integration of seismic profiles and industry wells, five shelf-margin clinothems are recognized in the late-Quaternary Pearl River shelf-margin sedimentary prism, named SQ1-SQ5 from chronologically oldest to youngest (Lin, He, et al., 2018; Lin, Jiang, et al., 2018; Liu et al., 2019, 2022; Ludmann et al., 2001; Wang et al., 2020) (Figure 1b). They represent five regressive-to-transgressive cycles and are bounded by six sequence boundaries: SB1-SB6. Based on the constraints of thermos-luminescence ages and paleontological markers and the assumption that basinwide unconformities represent significant periods of sea-level fall, Liu et al. (2019, 2022) and Wang et al. (2020) interpreted those unconformities to have formed during the most pronounced eustatic sea-level fall of MIS54, MIS38, MIS 20, MIS 12, MIS6, and MIS2 (Figure 1c). Those sea-level falls along with the sufficient sediment supply on the late-Quaternary Pearl River margin led to the regional regression and the subaerial exposure of the shelf and ultimately gave rise to the formation of unconformities. This paper focusses on the SQ3 and SQ4 to explore the growth of the shelf-margin clinothem, whose boundaries, SB3-SB5, are respectively dated as 795 ka (MIS 20), 440 ka (MIS 12), and 140 ka (MIS 6) (red lines in Figure 1b,c) (Lisiecki & Raymo, 2005; Liu et al., 2019; Miller et al., 2020; Wang et al., 2020).

2.2 | Previous work on the SQ3 and SQ4 shelf-margin clinothems

Using high-resolution seismic data, Gong et al. (2018), Gong, Qi et al. (2019) and Qi et al. (2022) mapped the detailed anatomy for SQ3 and SQ4. The anatomy suggested that on the whole Pearl River margin the SQ3 and SQ4 clinothems present significant differences, each of which has a distinct shelf edge trajectory and a given style of deep-water deposition (Figure 2 and Figure S1). Firstly, shelf-edge trajectories of those two clinothems were mapped out by linking shelf edges on two successive clinoforms. As shown in Figure 2b,c, SQ3 have a slight-rising trajectory, whereas SQ4 present a steep-rising one. Secondly, the deposition at the outlying deep-water reaches of those two clinothems were also characterized. SQ4 is composed of high-amplitude, continuous reflections whereas SQ3 shows chaotic and transparent reflections (Figure 2b–d). Therefore, SQ3 is characterized by fan lobes consisting mainly of MTDs whereas SQ4 is featured by traditional fan lobes consisting mainly of turbidites.

In addition, previous studies also mapped systems tracts at the outer-shelf segment of SQ3 and SQ4 from seismic data (Lin, He, et al., 2018; Lin, Jiang, et al., 2018). In Figure 2c and Figure S1, expressions of different systems tracts around the shelf edge are clearly presented; they reflect basic characteristics of

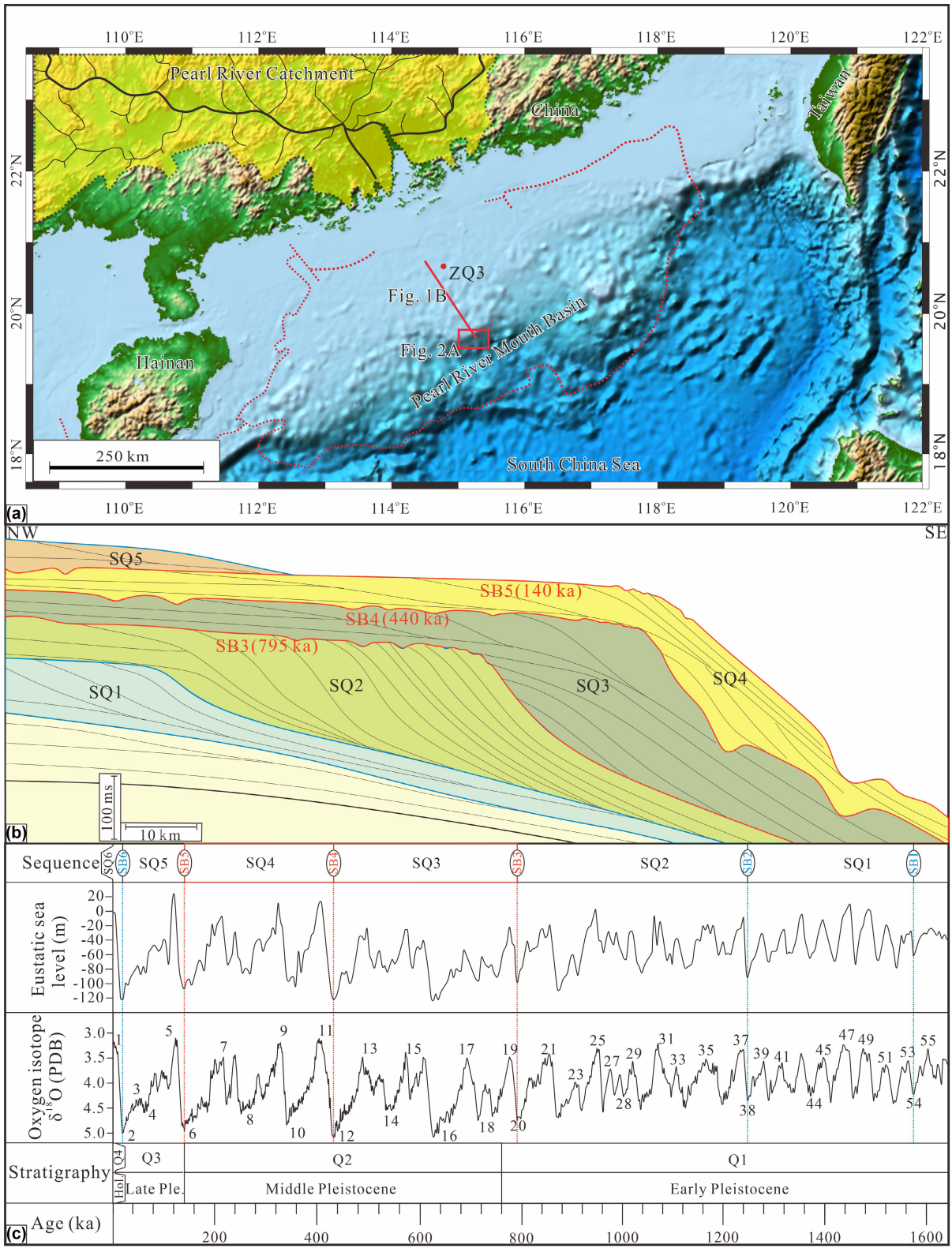

FIGURE 1 (a) Map of the northern South China Sea showing the geographic context of the Pearl River margin. Also shown are the plan-view locations of a cross section presented in b and a bathymetric map presented in Figure 2a. (b) A NW-SE trending regional cross section showing the sequence stratigraphic framework of the late-QAuaternary Pearl River margin (modified from Liu et al. (2019) and Wang et al. (2020)). (c) Age constrains of the sequence boundaries using oxygen isotope records of Lisiecki and Raymo (2005) and eustatic sea level curve of Miller et al. (2020) (modified from Liu et al. (2019, 2022)). Noted that SQ3 and SQ4 are the target clinothems of this study, which are bounded by SB3, SB4, and SB5, dated as 795, 440, and 140 ka respectively.

the cross-shelf transit of deltaic systems during the building of SQ3 and SQ4 and there are several points that should be noted. Firstly, lowstand systems tracts (LST) are occurred downdip of the pre-existing shelf edge (Figure 2c). Therefore, it is deduced that at the very start of a sea-level rise, deltaic systems have already advanced over the shelf-slope break. Secondly, transgressive systems tracts (TST) are rarely developed and relatively hard to be recognized in both SQ3 and SQ4 (Figure 2c). It indicates that the transit of deltaic systems to landward reaches of the continental margin seems to be a rapid process. Thirdly, highstand systems tracts (HST) are occurred around the shelf edge (Figure 2c). This suggests during sea-level highstand, deltaic systems can still prograde far out towards the outer shelf. Furthermore, HST is characterized by relatively flat top boundary throughout the study area (Figure 2c), indicating during that period deltaic systems have little amounts of aggradation. Lastly, forced regressive systems tracts (FST) are less developed within SQ3, with only a small part being recognized in the downdip area (Figure 2c). Therefore, the forced regression of deltaic systems at the end of SQ3 building also seems to be a rapid process.

3 | METHODS

3.1 | Dionisos

Dionisos is a stratigraphic forward model developed by IFPEN (Granjeon & Joseph, 1999). It uses a nonlinear sediment transport law and overland water flow routing (Granjeon, 1996, 2014; Granjeon & Joseph, 1999) to model erosional and depositional processes that have been observed in sediment transport models and modern systems (Coulthard & Van De Wiel, 2007; Syvitski & Milliman, 2007; Tucker & Slingerland, 1994). For each time step, Dionisos calculates three physical processes, namely the creation of accommodation (a function of eustasy, subsidence and compaction), sediment supply (a function of sediment discharge and water discharge), and the process of erosion, transport, and deposition of sediment. Modelling this combination of processes allows experimental simulation of the impacts of geological factors on the architecture and the volumes of depositional systems developed on basins scale over geological time scale (Harris et al., 2016, 2018, 2020; Hawie et al., 2018, 2019; Kovács et al., 2021). Therefore, DionisosFlow2016 has been employed herein to explore the relative sea-level control on the growth of shelf edges and the condition of sediments transporting into deep water.

3.2 | Model setup

To investigate the building of the individual clinothem within one relative sea-level cycle, we use the general geological condition of the late-Quaternary Pearl River margin and the common characteristics of SQ3 and SQ4 as references to constrain the values of input parameters and then setup a series of modelling experiments.

3.2.1 | Model grid dimensions and initial topography

As stated above, the studied SQ3 and SQ4 are bounded by unconformities dated as 795, 440, and 140 ka respectively (Figure 1), indicating that the fundamental time scale of the Pearl River margin sequences is likely to be around three hundred thousand years. We herein set model experiments spanning 340 ky, with 5 ky time steps (Table 1). Moreover, because this work mainly aims to investigate the relative sea-level control on the building of shelf-margin clinothems and that sea level can only practically be described as a one-dimensional time series, a mismatch in dimension space would be created when relating three-dimensional growth of clinothems to sea-level changes, making the comparison between model inputs and outputs very hard. Therefore, in this study we follow the classic sequence stratigraphic conceptual models (two-dimensional conceptual models) and assume strata on the continental margin have relatively consistent and laterally persistent stacking at the systems tract scale. As a result, "two-dimensional" stratigraphic forward modellings were conducted to simulate the growth of shelf-margin clinothems along depositional dip; the model dimensions are 410 km (depositional dip direction) by 20 km (depositional strike direction) with 10 km grid point spacing (Figure 3, Table 1). Furthermore, such modelling in the "two-dimensional" setting has other advantages. It not only reduces the computation time significantly but also filters out the autogenic processes along the strike of the shelf (Burgess et al., 2008; Harris et al., 2016, 2018, 2020; Kovács et al., 2021; Madof et al., 2016), avoiding the modelled results being biased.

Our Dionisos models were run on a typical shelf-slope topography, which has a total relief of 4300 m (Figure 3). The widths of the shelf and the slope are respectively 200 and 210 km, with gradients of 0.06° (1 m/km) and 1.2° (20 m/km) (Figure 3). Such values of the initial bathymetry are similar to those of the present Pearl River margin (Chen et al., 2012; Feng et al., 1996; Wang et al., 2020; Zhuo et al., 2015). Due to lowstand systems tracts (LST) of SQ3 and SQ4 both occurring downdip of the shelf-slope break (Figure 2c), deltaic systems have already prograded

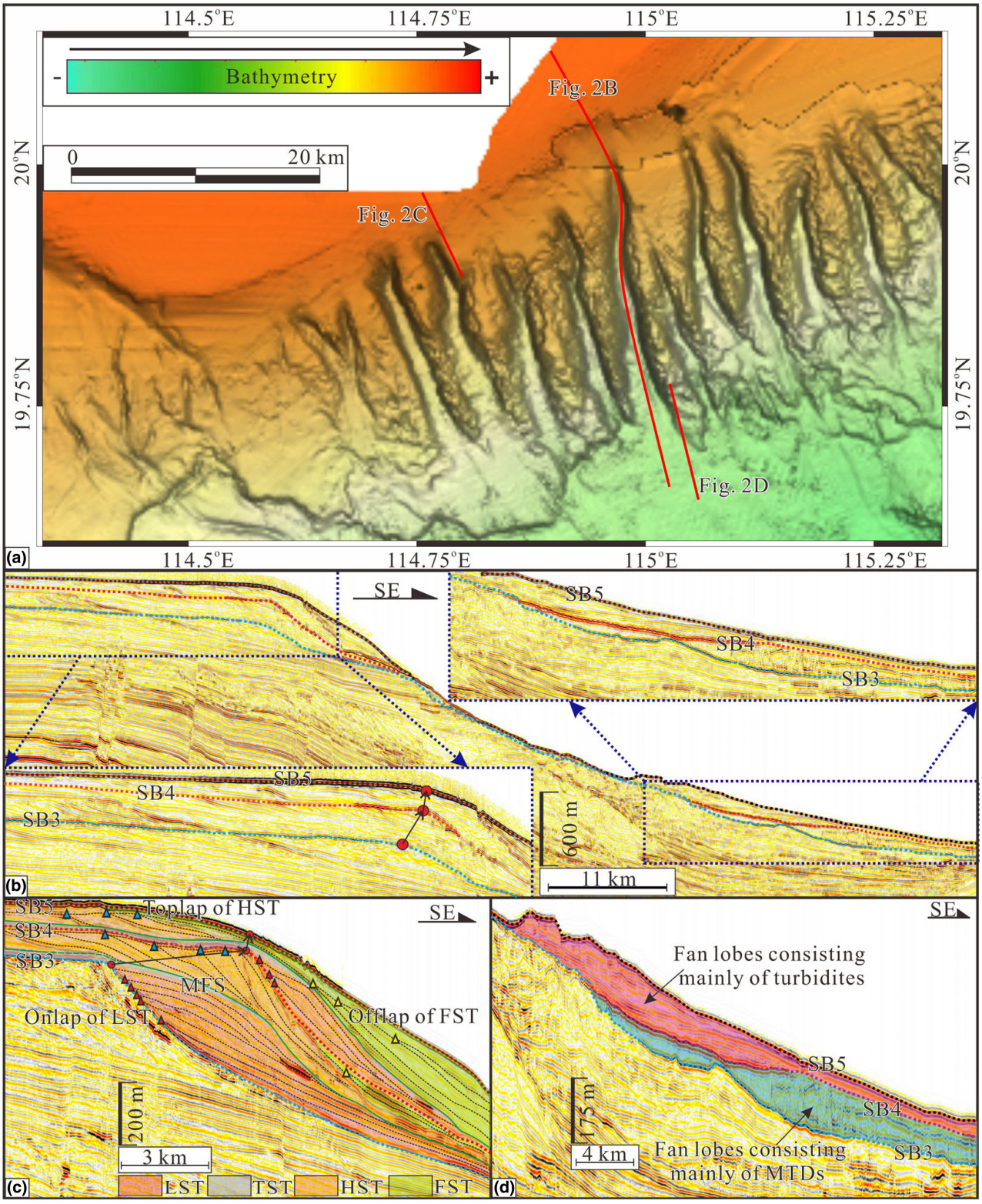

FIGURE 2 (a) Bathymetric map of the outer-shelf and slope segments of the Pearl River margin. The plan-view locations of seismic transects presented in b–d are shown. (b) A dip-oriented seismic section with zoomed insets of shelf edge and outlying deep-water segments illustrating the overall stacking of the studied SQ3 and SQ4. (c) A seismic profile showing the distribution of different systems tracts around the shelf edge of SQ3 and SQ4. The interpretation of those different systems tracts is referred from Lin, He, et al. (2018) and Lin, Jiang, et al. (2018). Moreover, for LST, HST and FST, their diagnostic reflection terminations of onlaps, toplaps and offlaops are respectively labelled by red, blue, and yellow triangles. (d) A seismic section spanning the deep-water reach of SQ3 and SQ4. Fan lobes at the mouth of canyons are clearly shown. For uninterpreted seismic profiles shown in b–d, please see the Figure S1. MFS, maximum flood surface.

farther than the pre-existing shelf-slope break at the very start of a rising-falling relative sea-level cycle. Therefore, we set the initial shoreline to be 50 m below the shelf edge (Figure 3). That is, the initial bathymetry value of the shelf edge and the proximal end are respectively −50 and −250 m (Figure 3).

TABLE 1 A summary of input parameters in each model

Parameter	Value
Domain length (*x* axis) (km)	410
Domain length (*y* axis) (km)	20
Grid spacing (km)	10
Run period (Ma)	0.34–0
Time steps (ky)	0.005
Sediment supply (km^3/My)	5000
Water discharge (m^3/s)	1200
Composition of sediment supply (sand, mud) (%)	20, 80
Amplitude of RSL change (m)	250
Gradient of initial shelf (°)	0.06
Gradient of initial slope (°)	1.2
Substrate thickness (m)	50
Gravity-driven terrestrial diffusion for mud (km^2/ky)	0.001
Gravity-driven terrestrial diffusion for sand (km^2/ky)	0.001
Gravity-driven marine diffusion for mud (km^2/ky)	0.001
Gravity-driven marine diffusion for sand (km^2/ky)	0.001
Water-driven terrestrial diffusion for mud (km^2/ky)	4000
Water-driven terrestrial diffusion for sand (km^2/ky)	1000
Water-driven marine diffusion for mud (km^2/ky)	10
Water-driven marine diffusion for sand (km^2/ky)	2
m	1.3
n	1.5
Relative duration of the HEST period (month)	3
HEST/LELT water discharge ratio	10
Critical slope failure (m/km)	26
Maximum erosion rate of sediment (m/My)	100

Abbreviations: HEST, high-energy short-term transport model; LELT, low-energy long-term transport model.

3.2.2 | Sediment supply and relative sea-level changes

As stated in Section 2.2, highstand systems tracts within both SQ3 and SQ4 can occur around the shelf edge (Figure 2c), which means deltaic systems could prograde onto the outer shelf during sea-level highstand. Therefore, sediment supply in our models must be sufficient enough to fill the shelf accommodation and facilitate the shoreline regression across the shelf to reach the outer shelf (Burgess & Hovius, 1998; Carvajal & Steel, 2006). Such high supply scenario of the Pearl River margin is consistent with the Quaternary uplift of the drainage area related to the Yundian Uplift of the Tibetan Plateau (Wang et al., 2011; Zhong & Ding, 1996) and the intensification of the East Asia Monsoon over the last 0.9 My (Clift et al., 2014; Metivier et al., 1999; Zhang et al., 2001). We herein apply a sediment supply rate of 5000 km^3/My and a water discharge value of 1200 m^3/s in all model runs, with the sediment load composed of 20% sand and 80% mud (Table 1). Those values are typical of modern large-sized fluvial systems (Milliman & Farnsworth, 2011), as shown in Figure S2. Furthermore, these values generate similar stratal geometries to those documented in seismic profiles of our previous studies (Gong et al., 2018; Gong, Qi, et al., 2019; Qi et al., 2022).

As for curves of relative sea levels, their values are set to have linear change fashions and their amplitudes are set to be constant in this study for simplifying sake (Figure 4). Ludmann et al. (2001) and Liu et al. (2019) used the depths of the offlap break of each delta front below present-day sea level to represent the values of relative sea level on

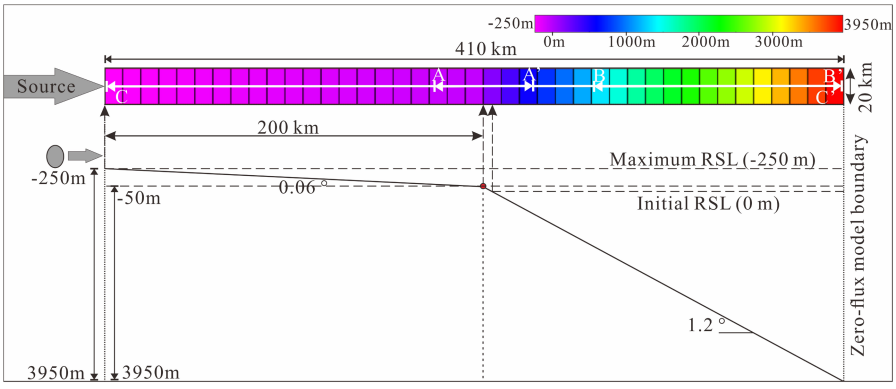

FIGURE 3 Initial bathymetry of Dionisos models in this study. It is shown both in the map view (top) and the cross section (below). Note that the initial relative sea level is 50 m below the shelf-slope break (the red dot). Map view shows the locations of cross sections of A-A′ in Figure 5d, B-B′ in Figure 7b, and C-C′ in Figures 10 and 11. RSL, relative sea level.

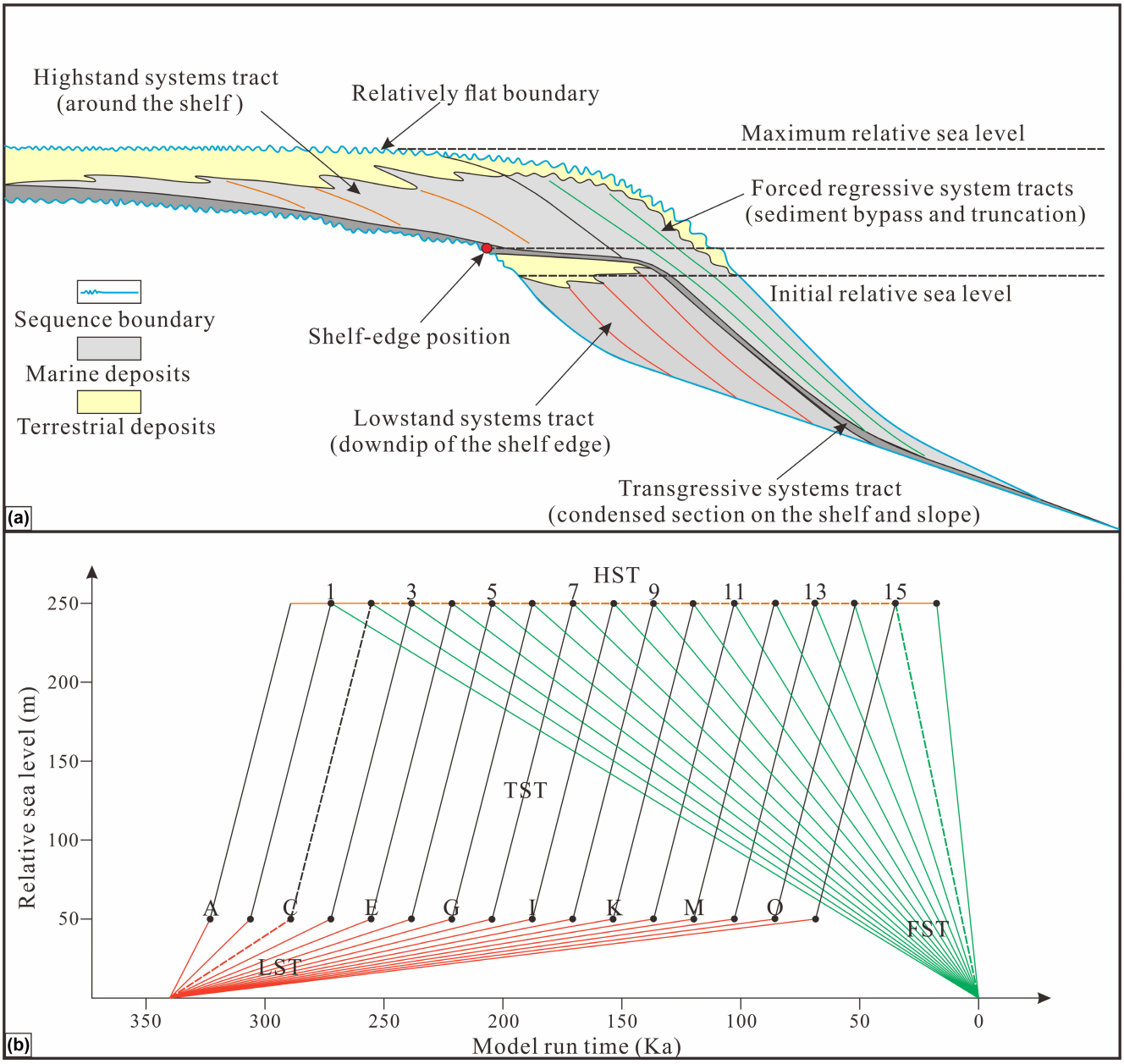

FIGURE 4 (a) A sketch diagram mapped from Figure 2c and showing the emplacement of different systems tracts within the shelf-margin clinothem. (b) Histories of relative sea levels used in the modelling. Their linear changes during LST, TST, HST, and FST that are shown in (a) are represented by red, grey, orange, and green lines respectively. Note that the same duration of TST (*T_TST*) were applied in each experiment, which correspond to a rise of sea level of 200 m and account for 10% of the elapsed model run (340 ky). However, for sea-level changes during LST, HST and FST, though they have the same variation amplitudes (50, 0, and 250 m respectively), their durations (*T_TST*, *T_HST*, and *T_FST*) range from 5% to 80% of the elapsed model run, with an increment of 5%. In this study, we suppose variations in *T_LST* and *T_FST* to be represented by letters A-P and numbers 1–16 respectively and there are totally 136 combinations, that is, 136 individual model runs. For example, in model C15, *T_LST*, *T_HST*, and *T_FST* respectively account for 15%, 65% and 10% of the elapsed model run, as highlighted by the dashed line.

the late-Quaternary Pearl River margin. Though these results should be regarded as an approximation because of the paucity of data and the fact that sediment loading, compaction and erosion have not been taken into consideration, they can still reflect the overall amplitude of the relative sea-level change to some degree. It was found that the delta fronts formed 795 and 440 ka lie today at water depths of 287 and 221 m, respectively (Liu et al., 2019; Ludmann et al., 2001). Therefore, we consider the overall amplitude of the relative sea-level change in our models as 250 m (Figures 3 and 4). According to the observations of SQ3 and SQ4 that LST collectively occur downdip of the

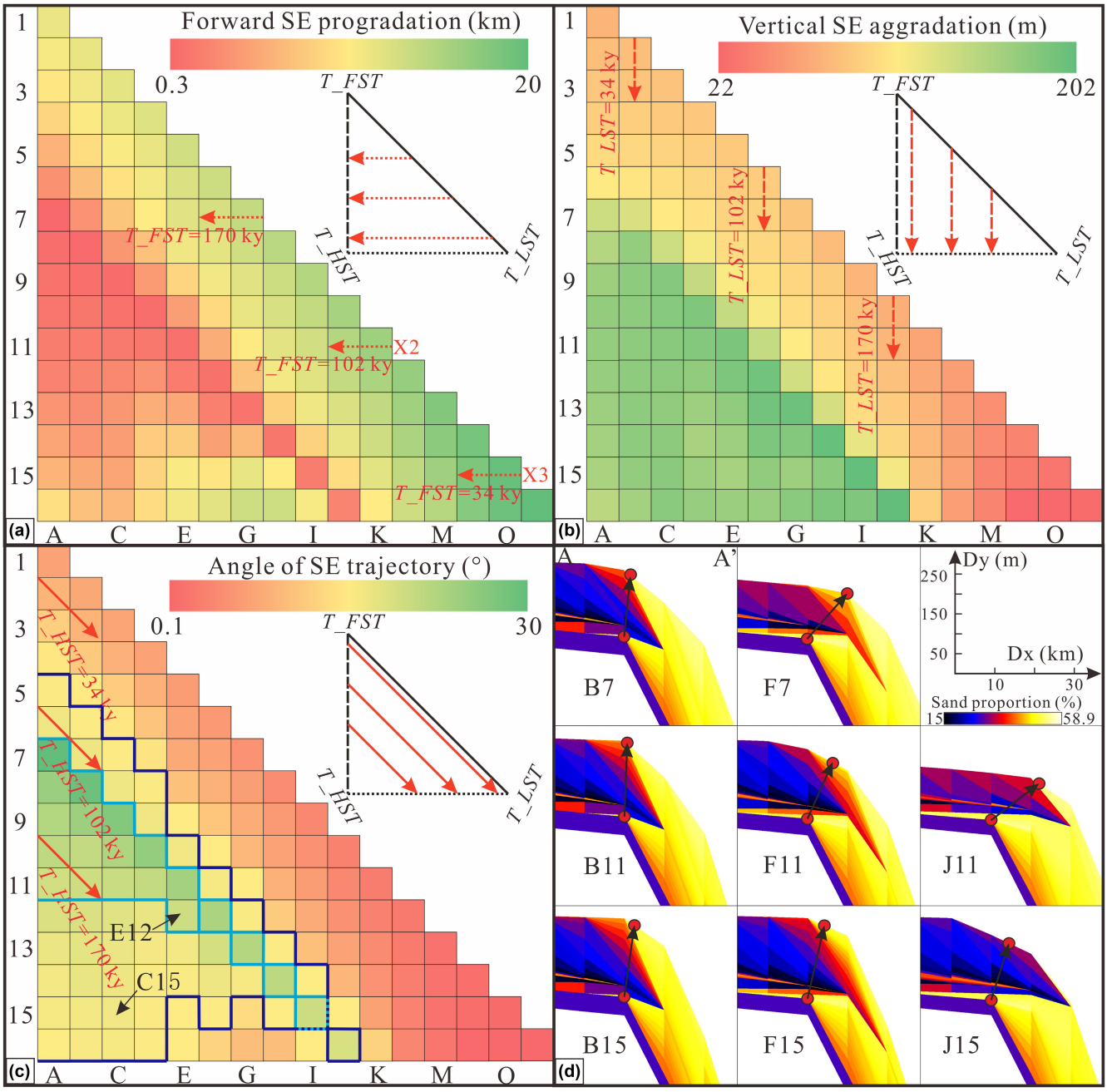

FIGURE 5 (a–c) Progradational components (*dx*), aggradational components (*dy*), and trajectory angles (α_{se}) of shelf-edge trajectories in clinothems produced by 136 models after 340 ky of simulated time. Values of those three kinds of parameters are indicated by associated colour bars. Note that within the model set, along the horizontal (dotted line), vertical (dashed line), and oblique (solid line) directions, *T_FST*, *T_LST* and *T_HST* are remained as constant, respectively. Furthermore, in each direction, three model series of *T_FST*, *T_LST* and *T_HST* remaining as 170, 102 and 34 ky are selected to be quantitatively shown in Figure 6. For the models bounded by dark and blue lines in c, they respectively refer to the model counterparts of SQ3 and SQ4, which are constrained by the real shelf-edge trajectories on the late-Quaternary Pearl River margin (Table S1). (d) Several 2-D stratigraphic cross sections around the shelf-edge areas (profile A-A' in Figure 3) showing the overall variations of shelf-edge trajectories (black arrows) within the model set. Note that only the cross sections of models corresponding to intersections of the selected horizontal and vertical model series are presented and that those sections are coloured by the sand proportion.

shelf-slope break as stated above (Figures 2c and 4a), the rise of relative sea level during lowstand should not exceed the initial bathymetry of the shelf edge (−50 m) (Figure 3). Therefore, the rise of relative sea levels during LST are set as 50 m and then the rise of TST are 200 m (Figure 4b). On the other hand, due to the top boundaries of HST within SQ3 and SQ4 are relatively flat (Figures 2c and 4a), the rise of relative sea level during highstand should be very

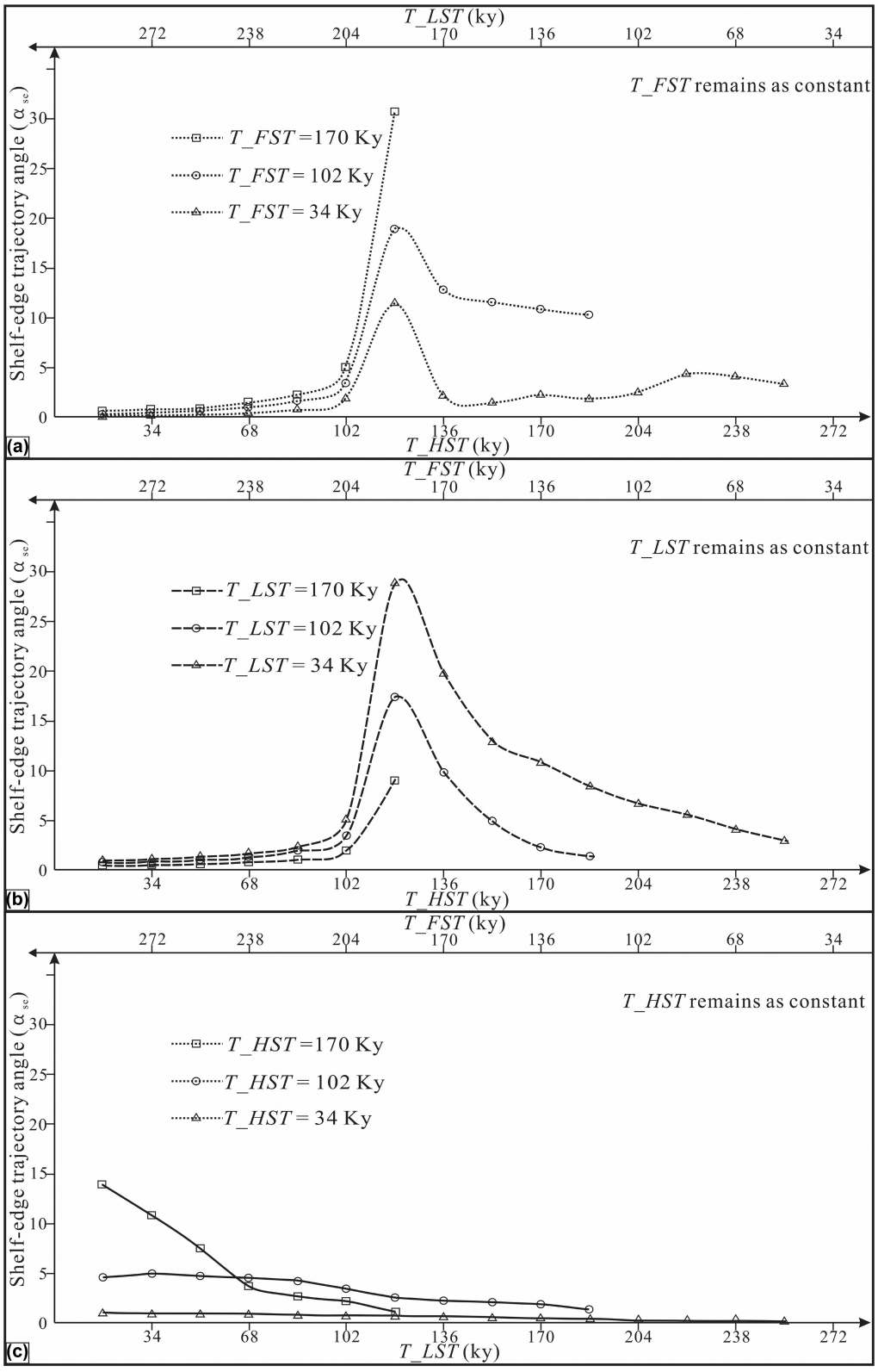

FIGURE 6 Variations of shelf-edge trajectory angles (α_{se}) when *T_FST* (a), *T_LST* (b), and *T_HST* (c) are respectively remained as constant. Note that under each scenario, α_{se} values of three model series of *T_FST*, *T_LST* and *T_HST* remaining as 170, 102, and 34 ky are selected to be shown and they are pointed out by dotted, dashed, and solid red arrows in Figure 5a–c.

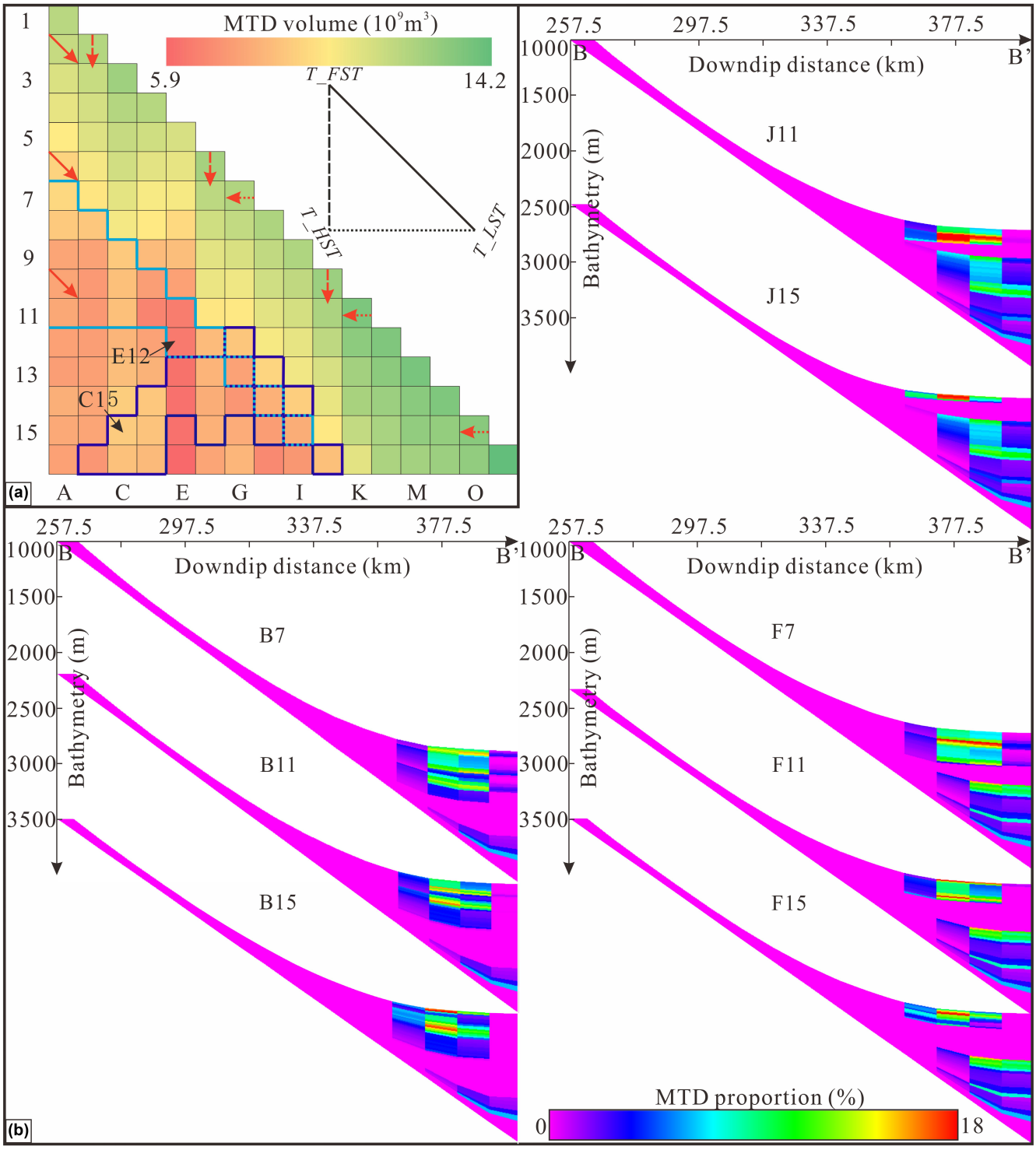

FIGURE 7 (a) Volumes of MTDs in deep-water areas (below the 1000 m isobath of the initial topography) of shelf-margin clinothems produced by 136 models. For the description of variations in MTDs volumes within the model set, the horizontal (dotted line), vertical (dashed line), and oblique (solid line) directions that respectively represent *T_FST*, *T_LST* and *T_HST* remaining constant are also used. (b) Several 2-D stratigraphic cross sections around the deep-water areas (profile B-B′ in Figure 3) showing the overall variation of MTD volumes within the model set. Note that due to the block of zero-flux boundaries at the distal end of our models, the stratal stacking patterns shown here are in fact artefacts.

limited, driving no accommodation for the aggradation of deltaic systems. Therefore, the rise of relative sea levels during HST are set as 0 m (Figure 4b).

As the only variable in our model set, relative sea-level conditions consistently change among different experiments. Those changes are concentrated on the durations

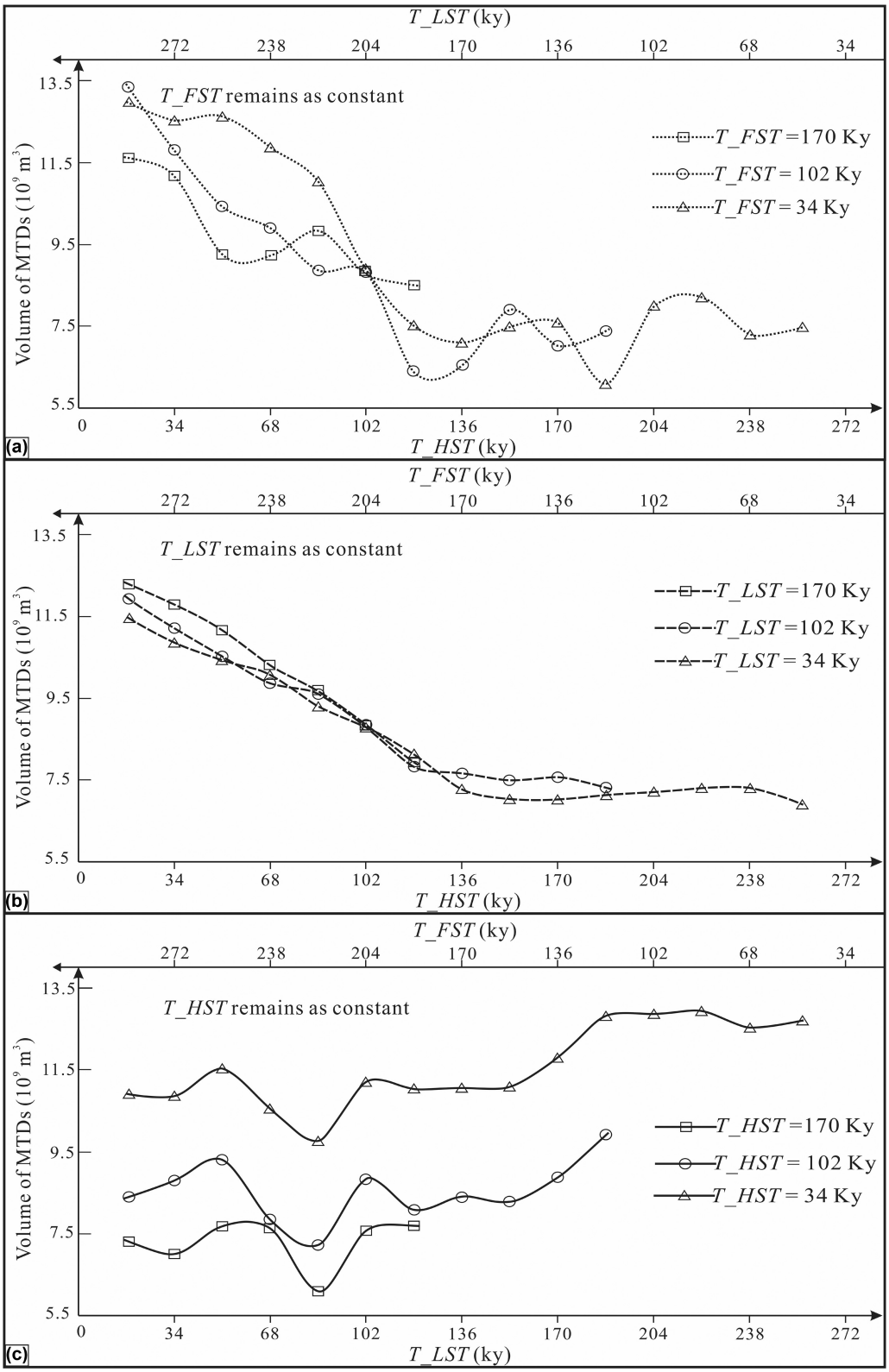

FIGURE 8 Variations of the volumes of MTDs when *T_FST* (a), *T_LST* (b), and *T_HST* (c) are respectively remained as constant. Under each scenario, volume values of the same three model series of *T_FST*, *T_LST* and *T_HST* remaining as 170, 102, and 34 ky are selected to be shown.

of LST, HST, and FST, which are respectively abbreviated as *T_LST*, *T_HST* and *T_FST* in this study (Figure 4b). Due to the rare development of TST (Figure 2c) and the deduction that transit of shoreline systems to landward reaches of the Pearl River margin seems to be a rapid process, *T_TST* is set to account for 10% of the elapsed model

run (34 ky) in each experiment (Figure 4b). However, for *T_LST*, *T_HST* and *T_FST*, their values range from 5% to 80% of the elapsed model run (17–272 ky), with an increment of 5% (17 ky) (Figure 4b). We herein suppose those variations in *T_LST* and *T_FST* to be represented by letter series of A-P and number series of 1–16, respectively and totally there are 1+2+3+4 ...+16 = 136 combinations, that is, 136 individual model experiments (Figure 4b). For example, for model C15 that is highlighted by the dashed line in Figure 4b, *T_LST*, *T_HST*, and *T_FST* respectively account for 15%, 65%, and 10% of the elapsed model run, that is, 51, 221, and 34 ky, respectively.

3.2.3 | Sediment transport parameters

Sediment transport in Dionisos is determined by a long-term hillslope creeping equation and short-term nonlinear continental and marine water driven equation:

$$Q_s = K_c S + K_w\, {q_w}^n\, S^m,$$

where Q_s is sediment flux, K_c and K_w are, respectively, the gravity- and water-driven diffusion coefficient, q_w is the water flux, n and m are exponents with values between 1 and 2 that affect sediment transport capacity, and S is the local slope (Granjeon, 2014; Tucker & Slingerland, 1994). All of these sediment-transport input values are listed in Table 1 and are set within the range of values used in other applications of diffusion-based modelling (Table 1) (Csato et al., 2013; Gong et al., 2021; Harris et al., 2016, 2018, 2020; Prince & Burgess, 2013). Perhaps more importantly, the modelled results suggest the selected diffusion coefficient are reasonable because resulting stratal geometries are similar to those documented in seismic profiles of our previous studies (Gong et al., 2018; Gong, Steel, et al., 2019; Qi et al., 2022).

3.3 | Model output

In order to systematically investigate relative sea-level forcings on the building of individual shelf-margin clinothems, Dionisos had been run 136 times to generate clinothems over a range of sea-level conditions (Figure 4b). In this study, we summarized (1) the growth of shelf edges and (2) the condition of sediments transporting into deep water. The growth of shelf edge is mainly characterized by the trajectories of shelf edges, which are mapped through linking the recognized shelf edges (areas of rollovers between the flat topset and the slope) on two successive shelf-margin clinoforms (Olariu & Steel, 2009; Zhang et al., 2017). Quantitatively, those shelf-edge trajectories are calculated from:

$$\alpha_{se} = \arctan\,(dy\,/\,dx),$$

where α_{se} is the trajectory angles, and dx and dy are the progradational and aggradational components of a given shelf-edge trajectory, respectively.

The condition of sediments transporting into deep water is proxied by the volumes of sediments initiated from mass-wasting processes, that is, mass-transport deposits (MTDs). We herein counted the volumes of MTDs in water below the 1000 m isobath of the initial topography. This depth is consistently below the deltaic systems throughout the model run and exactly corresponds to the water depth of present-day fan-lobe deposits on the Pearl River margin (Figure 2) (Chen et al., 2012; Feng et al., 1996; Wang et al., 2020; Zhuo et al., 2015). Within the clinothem generated in each model run, MTDs are exclusively resulted from the failures of sediments that have a gradient of more than 1.5° (26 m/km) (Table 1). Such value of the critical slope failure is consistent with the work of Wang et al. (2017), who characterized the two main phases of Quaternary MTDs on the Pearl River margin and found that their basal failure planes have gradients of 0.8°–2.3°. Moreover, that value is typical of submarine landslides on the world's continental margins, as shown by the slope failure database of Hance (2003) (Figure S2). Those sediment failures represent autogenic processes and are not user controlled but occurred due to the nonlinear sediment transport and accumulation. Because all models incorporated zero-flux boundaries (Figure 3), preventing sediments from leaving the model domain and conserving mass, calculations of those volumes of MTDs should be accurate. However, it must be admitted that the existences of those zero-flux boundaries may in turn create the boundary effect. For two lateral boundaries of our models, their boundary effect may affect the flow pattern to some degree. However, in this study due to model runs have all been influenced by that boundary effect, we do not think it is responsible for the variations in shelf-edge trajectories and MTDs volumes of generated clinothems. As for zero-flux boundaries at the distal end of our models, their boundary effect is mainly expressed as creating the artificial stratal stacking, but fortunately, those artefacts have no influence on the model output either.

4 | MODEL RESULTS

4.1 | The growth of shelf edges

Generally, shelf-edge trajectories of those individual clinothems generated by 136 model runs have progradation components (dx) of 0.3–20 km (Figure 5a,d) and

aggradational components (*dy*) of 22–202 m (Figure 5b,d). Due to *dx* values are at least an order of magnitude larger than those of *dy*, angles of shelf-edge trajectories (α_{se}) are mainly contributed by the forward shelf-edge progradation and they have a range from 0.1° to 30° (Figure 5c,d).

As shown in Figure 5c where α_{se} values of the modelled clinothems are calculated and plotted in, when *T_FST* is remained as constant, with the increase of *T_HST*, α_{se} values tend to have significant changes that first show a rising trend before fall (Figure 6a). For a given *T_LST*, increasing *T_HST* also causes drastic change of α_{se} values, which is presented as a rising-then-falling trend as well (Figures 5c and 6b). However, it must be noted that when *T_FST* or *T_LST* is relative long, those variations of α_{se} values only show gradually rising trends, as shown in the upper-left and lower-right corner of Figure 5c and the two model series of *T_FST* and *T_LST* remaining as 170 ky in Figure 6a,b. On the other hand, if *T_HST* is constant, it is found that changing of *T_LST* or *T_FST* does not drive pronounced changes of α_{se} values (Figure 5c). For example, when *T_HST* remain as 170, 102, and 34 ky, no matter how *T_LST* and *T_FST* have changed, α_{se} values only have maximum changes of 12.7°, 3.2° and 0.9°, respectively (Figure 6c).

According to the calculation formula for the angle of shelf-edge trajectory and the fact that α_{se} values are mainly contributed by the forward shelf-edge progradation, variations of *dx* values within the model set are exactly opposite to the scenarios of α_{se}. That is, for a given *T_FST* or *T_LST*, if *T_HST* is increasing, then *dx* values present falling-then-rising trends (Figure 5a,d). As for the *dy* values of the modelled clinothems, they are calculated and plotted in Figure 5b. We find for a given *T_FST* or *T_LST*, with the increase of *T_HST*, *dy* values collectively show an overall increasing trend (Figure 5b,d). However, when *T_HST* remains as constant, variations of *T_LST* or *T_FST* do not result in significant changes of *dx* or *dy* values (Figure 5a,b,d).

4.2 | The condition of sediments transporting into deep water

Within those individual clinothems generated by 136 model runs, mass transport deposits (MTDs) that are deposited below the 1000 m isobath of the initial topography have volumes ranging from from 5.9×10^9 to 14.2×10^9 m^3, (Figure 7a). Within the model set, the variation trends of those MTDs volumes are also described when *T_FST*, *T_LST*, and *T_HST* are respectively remained as constant (Figures 7a and 8).

When *T_FST* is remained as constant, it is found that variations of *T_HST* results in significant changes of MTDs volumes in deep-water areas (Figures 7 and 8a). With the increase of *T_HST*, MTDs volumes show an overall falling trend, but their values rise slightly when the *T_HST* is rather long (Figures 7 and 8a). Similarly, if *T_LST* has a specific value, such negative correlation between volumes of MTDs and durations of HST is also presented (Figures 7 and 8b); furthermore, those very slight rise of MTDs volumes also show up when *T_HST* is rather long (Figures 7 and 8b). On the other hand, when assuming *T_HST* as constant, variations of *T_LST* or *T_FST* only cause very small changes of MTDs volumes (Figures 7 and 8c). For example, when *T_HST* remains as 170, 102 and 34 ky, fluctuations of *T_LST* or *T_FST* only drive the maximum change of MTD volumes of 0.38×10^9, 1.51×10^9 and 1.8×10^9 m^3, respectively (Figure 8c).

5 | MODEL CONSTRAINS

To constrain the results of 136 individual model experiments to the real SQ3 and SQ4 on the late-Quaternary Pearl River margin, (1) the growth of shelf edges (2) the development of systems tracts, and (3) the condition of sediments transporting into deep water of those modelled clinothems are compared with those of SQ3 and SQ4 that have already been quantitatively characterized in previous works (Table S1). Firstly, in term of the growth of shelf edges, values of *dx* and α_{se} are used as constraints. Because only one clinothem's growth is simulated in our model experiments, implications of the shelf exposure and the subsequent truncation on the shelf aggradation are not taken into consideration. Therefore, *dy* values of the modelled clinothems are not comparable with those of SQ3 and SQ4 that had gone through subaerial truncation and should not be used as the constraint in this study. According to our previous works (Gong et al., 2018; Gong, Steel, et al., 2019; Qi et al., 2022), SQ3 displays strongly prograding shelf-edge trajectories with 1 km < *dx* < 6 km and 2° < α_{se} < 10°, whereas SQ4 contains shelf edges that are strongly aggradational with 200 m < *dx* < 1 km and 10° < α_{se} < 30°. Based on those ranges of *dx* and α_{se} values, potential model counterparts of SQ3 and SQ4 are constrained, as those listed in Table S1. Furthermore, such constrains of the modelled results based on the shelf-edge trajectories of SQ3 and SQ4 clinothems are also shown in Figure 5c where model counterparts of SQ3 and SQ4 are respectively bounded by dark and blue lines.

Secondly, with respect to the development of systems tracts within clinothems, previous seismic interpretations (Lin, He, et al., 2018; Lin, Jiang, et al., 2018; Liu et al., 2019) suggest FST are least developed within SQ3. That is, for models corresponding to SQ3, *T_FST* should be shorter than *T_ LST* and *T_HST*, according to which a further constrain is conducted, as shown by what listed in

Table S1. It should be noted that such further constrains are only conducted for the model counterparts of SQ3 and that the results are also shown in Figure 7a where model counterparts of SQ3 are further bounded by dark blue lines. Lastly, for the condition of sediments transporting into deep water, differences of MTDs volumes between SQ3 and SQ4 are considered as the constraint. At the outlying deep-water reaches fan lobes within SQ3 have higher MTDs contents compared with SQ4. Based on that limiting condition, we generate all combinations of potential model counterparts of SQ3 and SQ4, rule out those ones where volume differences of MTDs do not satisfy the constraint, and finally get all combinations of potential model counterparts of SQ3 and SQ4, as listed in Table S1. Such constrains based on the characteristics of deep-water deposits are also shown in Figure 9 where colourful and grey model combinations respectively represent ones that satisfy or do not satisfy the constraint. Furthermore, because of the sharp differences in the composition of fan lobes between SQ3 and SQ4 (fan lobes consisting mainly of MTDs vs. fan lobes consisting mainly of turbidites), we select two models that have the largest differences in MTDs volumes to represent the real building of SQ3 and SQ4, that is, models C15 and E12 (Figures 5, 7, 9, and Table S1).

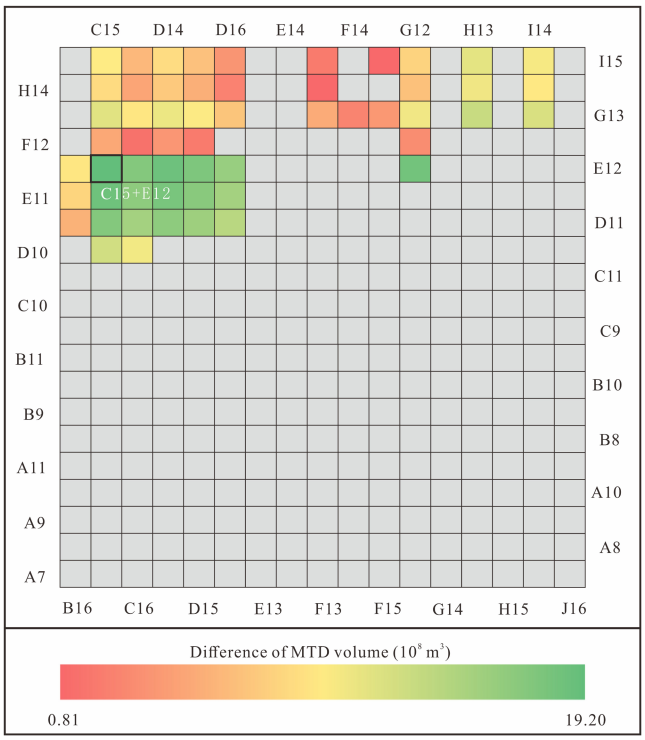

FIGURE 9 Model constrains according to the significant volume differences of MTDs between SQ3 and SQ4. All combinations of potential model counterparts of SQ3 and SQ4 are presented. Grey squares refer to combinations where volumes of MTDs do not satisfy the constraint. Colourful squares, however, represent combinations that satisfy the constraints, which are also listed in Table S1; their different colours indicate values of volume differences of MTDs between model counterparts of SQ3 and SQ4. A combination (C15+E12) that has the largest value of volume differences of MTDs is selected to reflect the real condition of the building of SQ3 and SQ4.

6 | GROWTH OF TWO DISTINCT SHELF-MARGIN CLINOTHEMS

As stated above, model C15 is selected to reflect the building of SQ3. Within that model, *T_LST*, *T_TST*, *T_HST* and *T_FST* last for 51, 34, 221 and 34 ky, respectively (Figure 4). After 340 ky of simulated time, the generated shelf trajectory has a progradational component of 2.5 km and an angle of 4.3° (Figure 5a,c). At the outlying deep-water reaches of the generated clinothem, MTDs have volumes of $8.2\times10^9\,m^3$ (Figure 7a). As shown in Figure 10a, for the growth of that clinothem, the relative duration of HST is quite long and the associated HST deposits span both the shelf and upper-slope segments. Furthermore, during the development of HST, the shoreline trajectory changes from a slight-rising trend to a steep-rising trend at the location of shelf edge (Figure 10b).

Model E12 is chosen to reflect the building of SQ4. Within that model, *T_LST*, *T_TST*, *T_HST* and *T_FST* are 85, 34, 136 and 85 ky, respectively (Figure 4). The output of this model suggests the generated shelf-edge trajectory has a progradational component of 0.9 km and an angle of 10.9° (Figure 5a,c). The volume of MTDs transported into deep water of the clinothem are $6.3\times10^9\,m^3$ (Figure 7a). As shown in Figure 10c, for the modelled clinothem, the relative duration of HST is comparable with LST and FST and the HST deposits are absent in the upper-slope segment. Moreover, during the development of HST, the shoreline trajectory shows a continuously slight-rising trend (Figure 10d).

In addition, to validate that models C15 and E12 are indeed reflecting the real condition of SQ3 and SQ4 building, the two models were successively run to generate two shelf-margin clinothems (Figure 11). However, it should be noted that the first running of C15 will generate a new topography that has a higher bathymetry at the proximal end (−312 m) compared with the initial bathymetry (−250 m) (Figure 11a). Therefore, for the subsequent running of model E12, we need to change its initial relative sea-level value from 0 to −62 m to ensure that the sea level can rise to the proximal end of the model (Figure 11a). After 680 ky of simulated time, the generated shelf-edge trajectory shows a clear transition from slight rising to steep rising (Figure 11b). Furthermore, distributions of different systems tracts within those two shelf-margin clinothems (Figure 11b) are very similar to those of SQ3 and SQ4 on the late-Quaternary Pearl River margin, as shown in Figure 2c.

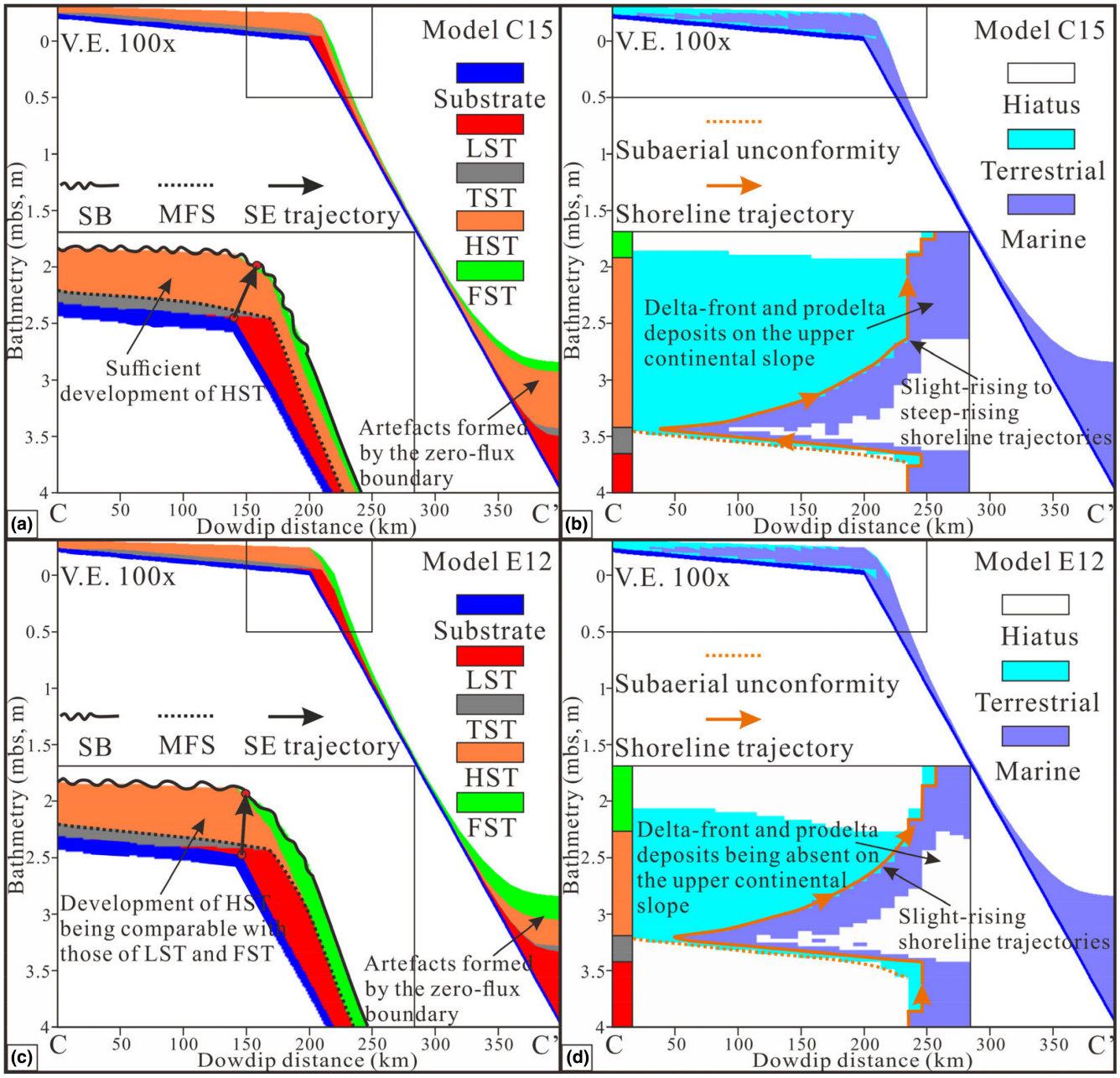

FIGURE 10 Cross sections (profile C-C′ in Figure 3) of model C15 (a,b) and E12 (c,d). Shelf-margin clinothems generated in those two models are presented in terms of the distribution of different systems tracts (a and c) and the distribution of different facies (b and d). The insets within the left and right panels respectively show the zoomed shelf-edge segments and the chronostratigraphic diagram of the shelf and the upper slope. Note that due to the block of zero-flux boundaries at the distal end of models, the stratal stacking patterns at the outlying deep-water reaches are in fact artefacts. MFS, maximum flood surface; RSL, relative sea level; SB, sequence boundary.

7 | DISCUSSION

7.1 | Relative sea-level control on the growth of shelf edges

As stated above, shelf-edge trajectories of individual clinothems generated in 136 model runs are the function of *T_LST*, *T_HST* and *T_FST* (Figures 5 and 6). Those correlations between systems tracts and shelf-edge trajectories reveal relative sea-level controls on the growth of shelf edges at the individual-clinothem scale of several 100 ky. Previous studies, however, mainly explained responses of the shelf-edge growth to the variation of relative sea levels over a time scale of 1 My or more; for example, a change in shelf-edge trajectories from flat to ascending was suggested to reflect the long-term change of relative sea levels from stable to rising (Gong, Steel, et al., 2019; Helland-Hansen et al., 2012; Helland-Hansen & Hampson, 2009). Within

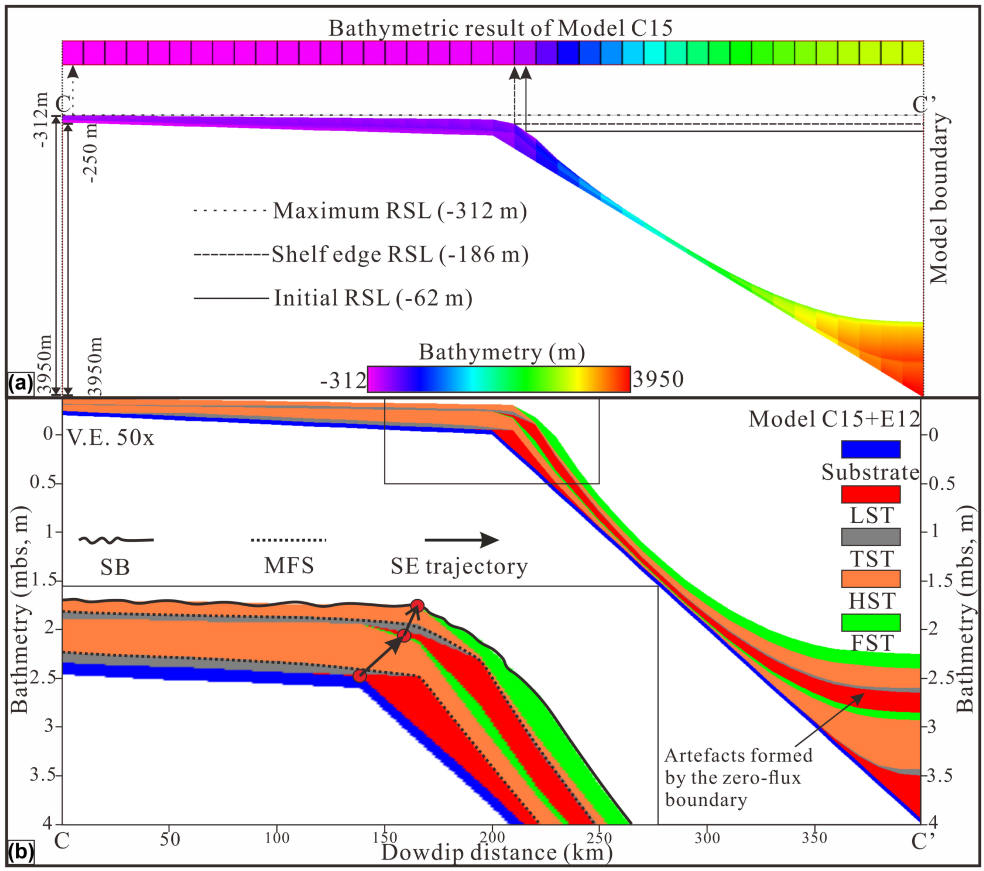

FIGURE 11 (a) Bathymetric result produced by model C15. It is shown in both the map view (top) and the cross section (below). Noted that after 340 ky of simulated time of model C15, the bathymetry has a maximum value of −312 m. To make sure the running of model E12 on such a bathymetry meet the model setup in this study, a bulk shift of the relative sea-level curve of model E12 is necessary and thus, we change the initial relative sea levels to −62 m. (b) Cross sections (profile C-C′ in Figure 3) of two shelf-margin clinothems generated by the successive running of two models: C15 and E12. Details about the presentation of those sections are same as those in Figure 10.

the model set, when *T_LST* or *T_FST* remains as constant, angles of shelf-edge trajectories show significant variations with changing *T_HST* (Figures 5 and 6a,b). Whereas, when *T_HST* remains unchanged, angles of shelf-edge trajectories only show slight variations with changing *T_LST* or *T_FST* (Figures 5 and 6c). Therefore, it is deduced that the growth of shelf edge is sensitive to the duration of HST relative to LST or FST. We think such a deduction on the tight relationship between the shelf-edge growth and the degree of HST development is exclusive on the late-Quaternary Pearl River margin, where a high supply-scenario was existed. Due to the Yundian Uplift of the Tibetan Plateau, the drainage area of the Pearl River was elevated in the late Quaternary (Wang et al., 2011; Zhong & Ding, 1996), which coupled with the intensification of the East Asia Monsoon since 0.9 Ma (Clift et al., 2014; Metivier et al., 1999; Zhang et al., 2001), significantly increase the sediment supply. Within the traditional sequence stratigraphy model, it is mainly during the periods of falling sea level and lowstands that terrestrial sediments are delivered to the shelf-margin staging area and drive the growth of the shelf edge (Mitchum, 1985; Vail et al., 1977; Van Wagoner et al., 1990). The development of LST and FST therefore commonly play more important roles on the growth of shelf edges. However, under the background of late-Quaternary Pearl River margin, during the sea-level highstand the sufficient sediment supply also drives the regression of shoreline systems across the shelf, facilitating the growth of the shelf edge. Therefore, within the model set of this study, the impacts of HST on the growth of shelf edges are significantly reinforced.

When *T_FST* or *T_LST* are remained as constant, the shelf-edge trajectory angles of clinothems show a rising-then-falling trend with the increase of *T_HST* (Figures 5 and 6a,b), Because of this, it is believed that there is a balance condition between the duration of HST and of LST or FST, in which *T_HST*, *T_LST* and *T_FST* are comparable and steep-rising shelf-edge trajectories would be formed. However, if the relative duration of HST is either very short or very long and thus does not reach or overreach that balance condition, slight-rising shelf-edge trajectories would be formed (Figures 5 and 6a,b). As shelf edges

are normally either fixed or basinward-accreting during the building of the shelf-margin clinothems (Gong, Steel, et al., 2019; Helland-Hansen & Hampson, 2009), those controls of systems tracts on the formation of high-angle versus low-angle ascending shelf-edge trajectories provide a useful method to predict the growth style of the shelf edge within the context of classic sequence stratigraphic conceptual models. However, it should be noted that the balance condition between the duration of HST and of LST or FST does not exist when the duration of another systems tracts is relatively long. For example, when *T_FST* remains as a relatively large value, shelf-edge trajectory angles only show a continuous rising trend with the increase of *T_HST*, as shown in the left upper corner of Figure 5c and the model series of *T_LST* remaining as 170 ky in Figure 6a. In this case, because most of the simulated time is concentrated on *T_FST*, *T_HST* is limited, which hinders it achieving or overreaching the balance condition with *T_LST*. Therefore, with the given sediment supply in the model, the development of HST only play a role to drive the increase of shelf-edge trajectory angles and facilitate the aggradation of the shelf edge.

Through the constrain of the model set to the real condition of the building of SQ3 and SQ4 on the late-Quaternary Pearl River margin (Figure 9 and Table S1), it is found that the slight rising shelf-edge trajectory of SQ3 corresponds to relatively long *T_HST* that has overreached its balance condition with *T_LST* or *T_FST* (Figures 5c and 10a). As shown in Figure 10a,b and the sketch diagram of Figure 12a, during the development of HST, deltaic systems prograded over the pre-existing shelf-slope break and delta-front and prodelta deposits draped down into the upper continental slope below. Such building processes widened the shelf, accreted the clinoform slope, and thus, gave rise to the formation of slight-rising shelf-edge trajectories. On the other hand, the steep-rising shelf-edge trajectory of SQ4 corresponds to the balance condition between the duration of HST and other systems tracts (Figures 5c and 10c). Under the circumstances, those highstand deltaic systems advanced to but do not over the early-existing shelf-slope break, with delta-front and prodelta deposits being absent on the upper continental slope (Figures 10c,d and 12b). Furthermore, subsequent deposits of FST directly perch on the continental

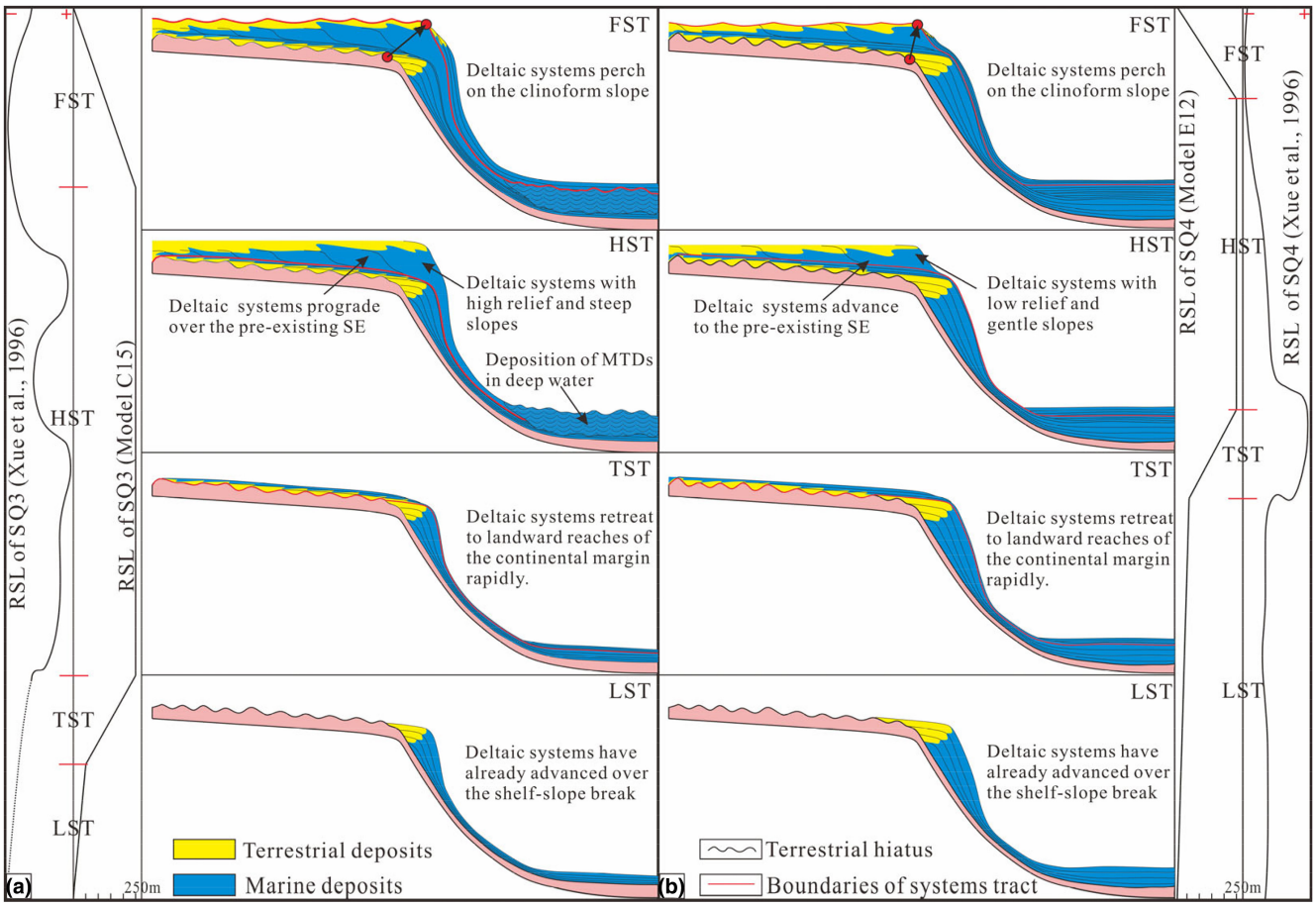

FIGURE 12 Sketch diagrams showing the gradual building of SQ3 (a) and SQ4 (b) with the successive development of LST, TST, HST and FST. Relative sea-level curves used in models C15 and E12 are also presented and it could be seen that they are similar to those from Xue et al. (1996).

slope (Figures 10b,c and 12b). Such building processes did not drive the significant accretion of the shelf edge and thus, resulted in the steep-rising shelf-edge trajectory (Figures 10b and 12b).

7.2 | Relative sea-level control on the condition of sediments transporting into deep water

On the continental margin, sediments are transported into deep water mainly through the form of feeding sediments directly into submarine canyons, or feeding them into slope either by mass-wasting processes or by hyperpycnal flows plunge (Covault & Graham, 2010; Jorry et al., 2008; Petter & Steel, 2006). As a result, the repetitive cycles of MTDs and turbidite deposits are found to have developed in deep-water areas around the world, like the Pleistocene intraslope basins of the western Gulf of Mexico (Beauboeuf & Friedmann, 2000), the offshore Trinidad and Tobago (Brami et al., 2000; Moscardelli et al., 2006), and the Adriatic Basin (Pellegrini et al., 2018). Our modelled results on MTDs volumes in deep-water reaches of clinothems therefore reflect relative sea-level controls on the condition of sediment transporting into deep water and they provide a useful method to predict the type of deep-water depositional elements over the individual-clinothem scale. Within the model set, when *T_LST* or *T_FST* is remained as constant, volumes of MTDs show significant decreases with the increase of *T_HST* (Figures 7 and 8a,b). Whereas when *T_HST* remains constant, volumes of MTDs only fluctuate slightly with the change of *T_LST* or *T_FST* (Figures 7 and 8c). It is suggested that the occurrence of mass-wasting process and the resultant deposition of MTDs are also sensitive to the duration of HST relative to LST or FST. Such argument can also be explained by the exclusive geological condition of high sediment supply and high relative sea-level amplitude on the late Quaternary Pearl River margin, as stated above.

When *T_FST* or *T_LST* are remained as constant, MTD volumes within individual clinothems present an overall falling trend with the increase of *T_HST* (Figures 7 and 8a,b). It is indicated that the development degree of HST generally play a negative role on the occurrence of MTDs in deep water. When *T_HST* lasts long enough and is comparable with *T_LST* or *T_FST*, MTD volumes tend to have small values, whereas if *T_HST* is quite shorter compared with *T_LST* or *T_FST*, MTDs tend to have large volumes (Figures 7 and 8a,b). In addition, it should be noted that when T_HST is rather long, there is a slight rise of MTDs volumes with the increase of *T_HST* (Figures 7 and 8a,b). With *T_HST* lasting far over *T_LST* or *T_FST*, MTD volumes in deep water can also have relatively large values. Through the constrain of the model set to the real condition of the building of SQ3 and SQS4 (Figure 9 and Table S1), it is found that fan lobes consisting mainly of MTDs of SQ3 correspond to the scenario where T_HST is dominated during the growth of clinothem (Figures 7a and 10a). Highstand deltaic systems prograded over the pre-existing shelf-slope break and delta fronts merged onto the continental slope, which in turn resulted in delta characteristics of high relief and steep slope (Figures 10a and 12a). Furthermore, due to the process of self-regulated equilibrium (Burgess et al., 2008; Harris et al., 2016, 2018), the stacking pattern of shelf-edge deltas changed from progradation to aggradation at the end of HST, as shown by the change of shoreline trajectory from slight rising to steep rising (Figure 10b). Such aggradation of shelf-edge deltas will reinforce their high relief and steep slope, cause the significant instability of the shelf-edge segment, and then drive the occurrence of mass wasting processes and the deposition of MTDs in deep water. On the other hand, fan lobes consisting mainly of turbidites of SQ4 correspond to the condition where the relative duration of HST is comparable with LST or FST (Figures 7a and 10c). In this case, because deltaic systems advanced to but did not over the early-existing shelf-slope break, the relatively shallow water environment on the shelf formed deltas with characteristics of low relief and gentle slope (Figures 10c,d and 12b). Therefore, the shelf-edge segment tended to be relatively stable, which disfavour the occurrence of sediment failure and the deposition of MTDs.

8 | CONCLUSION

1. Under the geological background of high sediment supply on the late-Quaternary Pearl River margin, Dionisos stratigraphic forward modelling experiments demonstrate that the duration of HST relative to LST or FST significantly affects the growth of shelf edges and the condition of sediments transporting into deep water over the individual-clinothem scale. Specifically, the much shorter or longer duration of HST relative to LST or FST tends to form slight-rising shelf-edge trajectories and large-volume MTDs in deep water, whereas the comparable durations of HST, LST, and FST tends to cause steep-rising shelf-edge trajectories and limited MTDs. Such relative sea-level controls on the building of the shelf-margin clinothem provide an effective method to predict the stacking pattern of shelf edges and the type of deep-water depositional elements over an individual-clinothem scale of several 100 ky.

2. On the late-Quaternary Pearl River Margin, progradational shelf edges and fan lobes consisting mainly of MTDs of SQ3 are caused by the rather longer duration of HST relative to LST or FST. During the building of SQ3, highstand deltaic systems advanced over the pre-existing shelf-slope break, which led to the significant accretion and instability of the shelf edge and thus, gave rise to the formation of slight-rising shelf-edge trajectories and the high contents of MTDs in deep water. On the other hand, aggradational shelf edges and fan lobes consisting mainly of turbidites of SQ4 were resulted from the comparable durations of HST, LST, and FST. During the building of SQ4, highstand deltaic systems advanced to but not over the early-existing shelf-slope break, which coupled with the subsequent perching of FST on the clinoform slope, did not drive the pronounced accretion and instability of the shelf edge and thus, caused the formation of steep-rising shelf-edge trajectories and the low contents of MTDs.

ACKNOWLEDGEMENTS

This research was jointly funded by the National Natural Science Foundation of China (Nos. 41972100 and 41802117) and the Science Foundation of China University of Petroleum, Beijing (No. 2462020YXZZ020). The authors thank the academic licence of DionisosFlow provided by the Beicip-Franlab. The authors are also grateful to journal editor (Dr. Cari Johnson) for editorial handing and comments and to three reviewers (Dr. Ádám Kovács, Dr. Didier Granjeon, and Dr. Ashley Harris) for their insightful and constructive comments, all of which significantly improved the overall quality of the current study.

CONFLICT OF INTEREST

No conflict of interest is declared.

PEER REVIEW

The peer review history for this article is available at https://publons.com/publon/10.1111/bre.12738.

DATA AVAILABILITY STATEMENT

The data used for the research described in this article are sensitive without an open-source online data repository. Please contact the corresponding author for the detailed information.

ORCID

Jinyu Zhang https://orcid.org/0000-0002-1440-3885

REFERENCES

Beauboeuf, R. T., & Friedmann, S. J. (2000). High resolution seismic/sequence stratigraphic framework for the evolution of Pleistocene intra slope basins, western Gulf of Mexico: Depositional models and reservoir analogs. In P. Weimer, R. M. Slatt, J. Coleman, N. C. Rosen, H. Nelson, A. H. Bouma, M. J. Styzen, & D. T. Lawrence (Eds.), *Deep-water reservoirs of the world: SEPM, Gulf Coast Section, 20th Annual Research Conference*, Houston, TX, 40–60.

Brami, T. R., Pirmez, C., Archie, C., Heeralal, S., & Holman, K. L. (2000). Late Pleistocene deep-water stratigraphy and depositional processes, offshore Trinidad and Tobago. In P. Weimer, R. M. Slatt, J. Coleman, N. C. Rosen, H. Nelson, A. H. Bouma, M. J. Styzen, & D. T. Lawrence (Eds.), *Deep-water reservoirs of the world: SEPM, Gulf Coast Section, 20th Annual Research Conference*, Houston, TX, 104–115.

Burgess, P., Steel, R. J., & Granjeon, D. (2008). Stratigraphic forward modeling of basin-margin clinoform systems: Implications for controls on topset and shelf width and timing of formation of shelf-edge deltas. *SEPM Special Publication*, *90*, 35–45.

Burgess, P. M., & Hovius, N. (1998). Rates of delta progradation during highstands: Consequences for timing of deposition in deep-marine systems. *Journal of the Geological Society*, *155*, 217–222.

Carvajal, C., Steel, R. J., & Petter, A. (2009). Sediment supply: The main driver of shelf margin growth. *Earth-Science Reviews*, *96*, 221–248.

Carvajal, C. R., & Steel, R. J. (2006). Thick turbidite successions from supply-dominated shelves during sea-level highstand. *Geology*, *34*, 665–668.

Catuneanu, O. (2019). Scale in sequence stratigraphy. *Marine and Petroleum Geology*, *106*, 128–159.

Catuneanu, O., Abreu, V., Bhattacharya, J. P., Blum, M. D., Dalrymple, R. W., Eriksson, P. G., Fielding, C. R., Fisher, W. L., Galloway, W. E., Gibling, M. R., Giles, K. A., Holbrook, J. M., Jordan, R., Kendall, C. G., Macurda, B., Martinsen, O. J., Miall, A. D., Neal, J. E., Nummedal, D., … Winker, C. (2009). Towards the standardization of sequence stratigraphy. *Earth-Science Reviews*, *92*(1–2), 1–33.

Chen, H., Cai, G., Luo, W., Wu, J., Huang, L., & Li, L. (2012). Features of canyon morphology and their origin in the Shenhu area, northern slope of the South China Sea. *Marine Geology and Quaternary Geology*, *32*, 19–26. [in Chinese].

Clift, P. D., Wan, S., & Blusztajn, J. (2014). Reconstructing chemical weathering, physical erosion and monsoon intensity since 25 Ma in the northern South China Sea: A review of competing proxies. *Earth-Science Reviews*, *130*, 86–102.

Coulthard, T. J., & Van De Wiel, M. J. (2007). Quantifying fluvial non linearity and finding self organized criticality? Insights from simulations of river basin evolution. *Geomorphology*, *91*(3–4), 216–235.

Covault, J. A., & Graham, S. A. (2010). Submarine fans at all sea-level stands: Tectonomorphologic and climatic controls on terrigenous sediment supply delivery to the deep sea. *Geology*, *38*, 939–942.

Csato, I., Granjeon, D., Catuneanu, O., & Baum, G. R. (2013). A three-dimensional stratigraphic model for the Messinian crisis in the Pannonian Basin, eastern Hungary. *Basin Research*, *25*, 121–148.

Feng, Z., Feng, W., Xue, W., Liu, Z., Chen, J., & Li, W. (1996). *Evaluation of marine geologic hazards and engineering geological conditions in the northern South China Sea* (p. 178). Hehai University Publishing House. [in Chinese].

Franke, D., Barckhausen, U., Baristeas, N., Engels, M., Ladage, S., Lutz, R., Montano, J., Pellejera, N., Ramos, E. G., & Schnabel, M. (2011). The continent ocean transition at the southeastern margin of the South China Sea. *Marine and Petroleum Geology*, *28*(6), 1187–1204.

Gong, C., Blum, M. D., Wang, Y., Lin, C., & Xu, Q. (2018). Can climatic signals be discerned in a deep-water sink? An answer from the Pearl River source-to-sink sediment-routing system. *GSA Bulletin*, *130*, 661–677.

Gong, C., Li, D., Steel, R. J., Peng, Y., Xu, S., & Wang, Y. (2021). Delta-to-fan source-to-sink coupling as a fundamental control on the delivery of coarse clastics to deepwater: Insights from stratigraphic forward modelling. *Basin Research*, *33*(6), 2960–2983.

Gong, C., Qi, K., Ma, Y., Li, D., Feng, N., & Xu, H. (2019). Tight coupling beweeen the cyclicity of deep-water systems and rising-then-flat shelf-edge pairs along the submarine segment of the Qiongdongnan sediment-routing system. *Journal of Sedimentary Research*, *89*, 956–975.

Gong, C., Steel, R. J., Wang, Y., Sweet, M. L., Xian, B., Xu, Q., & Zhang, B. (2019). Shelf-edge delta overreach at the shelf break can guarantee the delivery of terrestrial sediments to deep water at all sea-level stands. *American Association of Petroleum Geologists Bulletin*, *103*, 65–90.

Gong, C., Wang, Y., Zhu, W., Li, W., & Xu, Q. (2013). Upper Miocene to quaternary unidirectionally migrating deep-water channels in the Pearl River Mouth Basin, northern South China Sea. *AAPG Bulletin*, *97*(2), 285–308.

Granjeon, D. (1996). *Modélisation stratigraphique déterministe: Conception et applications d'un modèle diffusif 3D multilithologique* [Doctoral dissertation]. Université Rennes 1.

Granjeon, D. (2014). *3D forward modelling of the impact of sediment transport and base level cycles on continental margins and incised valleys. From depositional systems to sedimentary successions on the Norwegian continental margin* (pp. 453–472). John Wiley & Sons Ltd.

Granjeon, D., & Joseph, P. (1999). Concepts and applications of a 3D multiple lithology, diffusive model in stratigraphic modeling. In J. W. Harbough, W. L. Watney, E. C. Rankey, R. Slingerland, R. H. Goldstein, & E. K. Franseen (Eds.), *Numerical experiments in stratigraphy: Recent advances in stratigraphic and sedimentologic computer simulations* (Vol. *62*, pp. 197–210). SEPM, Special Publication.

Hance, J. J. (2003). *Development of a database and assessment of seafloor slope stability based on published literature* [Master Dissertation]. University of Texas at Austin.

Harris, A., Covault, J., Madof, A., Sun, T., Sylvester, Z., & Granjeon, D. (2016). Three-dimensional numerical modelling of eustatic control on continental-margin sand distribution. *Journal of Sedimentary Research*, *86*, 1434–1443.

Harris, A. D., Baumgardner, S. E., Sun, T., & Granjeon, D. (2018). A poor relationship between sea level and deep-water sand delivery. *Sedimentary Geology*, *370*, 42–51.

Harris, A. D., Covault, J. A., Baumgardner, S. E., Sun, T., & Granjeon, D. (2020). Numerical modeling of icehouse and greenhouse sea-level changes on a continental margin: Sea-level modulation of deltaic avulsion processes. *Marine and Petroleum Geology*, *111*, 807–814.

Hawie, N., Covault, J., Dunlap, D., & Sylvester, Z. (2018). Slope-fan depositional architecture from high-resolution forward stratigraphic models. *Marine and Petroleum Geology*, *91*, 576–585.

Hawie, N., Covault, J., & Sylvester, Z. (2019). Grain-size and discharge controls on submarine-fan depositional patterns form forward stratigraphic models. *Frontier in Earth Science*, *7*, 334.

He, M., Zhu, W., Wu, Z., Zhong, G., Ren, J., Liu, L., & Wang, W. (2019). Neotectonic movement characteristics and hydrocarbon accumulation of the Pearl River mouth basin. *China Offshore Oil Gas*, *31*, 9–20.

Helland-Hansen, W., & Hampson, G. (2009). Trajectory analysis: Concepts and applications. *Basin Research*, *21*(5), 454–483.

Helland-Hansen, W., Steel, R. J., & Sømme, T. O. (2012). Shelf genesis revisited. *Journal of Sedimentary Research*, *82*, 133–148.

Henriksen, S., Hampson, G. J., Helland-Hansen, W., Johannessen, P., & Steel, R. J. (2009). Shelf edge and shoreline trajectories, a dynamic approach to stratigraphic analysis. *Basin Research*, *21*, 445–453.

Johannessen, E. P., & Steel, R. J. (2005). Shelf-margin clinoforms and prediction of deepwater sands. *Basin Research*, *17*, 521–550.

Jorry, S. J., Droxler, A. W., Mallarino, G., Dickens, G. R., Bentley, S. J., Beaufort, L., Peterson, L. C., & Opdyke, B. N. (2008). Bundled turbidite deposition in the central Pandora trough (gulf of Papua) since last glacial maximum: Linking sediment nature and accumulation to sea level fluctuations at millennial timescale. *Journal of Geophysical Research*, *113*, F01S19.

Kovács, Á., Balázs, A., Špelić, M., & Sztanó, O. (2021). Forced or normal regression signals in a lacustrine basin? Insights from 3D stratigraphic forward modeling in the SW Pannonian Basin. *Global and Planetary Change*, *196*, 103376.

Li, S. T., Lin, C. S., Zhang, Q. M., Yang, S. G., & Wu, P. K. (1999). Episodic rifting dynamics of the continental marginal basins and tectonic events since 10 Ma in the South China Sea. *China Science Bulletin*, *44*, 9–22.

Lin, C., He, M., Steel, R., Zhang, Z., Li, H., Zhang, B., Wu, W., Shu, L., Tian, H., Zhang, X., Xing, Z., Wang, S., & Zhang, M. (2018). Changes in inner- to outer-shelf delta architecture, Oligocene to Quaternary Pearl River shelf-margin prism, northern South China Sea. *Marine Geology*, *404*, 187–204.

Lin, C., Jiang, J., Shi, H., Zhang, Z., Liu, J., Qin, C., Li, H., Ran, H., Wei, A., Tian, H., Xing, Z., & Yao, Q. (2018). Sequence architecture and depositional evolution of the northern continental slope of the South China Sea: Responses to tectonic processes and changes in sea level. *Basin Research*, *30*, 568–595.

Lisiecki, L. E., & Raymo, M. E. (2005). A Pliocene–Pleistocene stack of 57 globally distributed benthic δ18O records. *Paleoceanography*, *20*, PA1003.

Liu, H., Lin, C., Zhang, Z., Zhang, B., Jiang, J., Tian, H., & Liu, H. (2019). High-resolution sequence architecture and depositional evolution of the quaternary in the northeastern shelf margin of the South China Sea. *Acta Oceanologica Sinica*, *38*, 86–98.

Liu, H., Lin, C., Zhang, Z., Zhang, B., Tian, H., Zhang, M., & Jiang, J. (2022). Shelf-margin architecture and deposition variability across the mid-Pleistocene climate transition, northeastern South China Sea. *Marine Geology*, *443*, 106690.

Ludmann, T., Wong, H. K., & Wang, P. X. (2001). Plio-quaternary sedimentation processes and neotectonics of the northern continental margin of the South China Sea. *Marine Geology*, *172*(3–4), 331–358.

Madof, A. S., Harris, A. D., & Connell, S. D. (2016). Nearshore along-strike variability: Is the concept of the systems tract unhinged? *Geology*, *44*, 315–318.

Magyar, I., Krezsek, C., & Tari, G. (2019). Clinoforms as paleogeographic tools: Development of the Danube catchment above the deep Paratethyan basins in central and Southeast Europe. *Basin Research*, *32*, 320–331.

Mellere, D., Plink-Bjorklund, P., & Steel, R. J. (2002). Anatomy of shelf deltas at the edge of a prograding Eocene shelf margin, Spitsbergen. *Sedimentology*, *49*, 1181–1206.

Metivier, F., Gaudemer, Y., Tapponnier, P., & Klein, M. (1999). Mass accumulation rates in Asia during the Cenozoic. *Geophysical Journal International*, *137*, 280–318.

Miller, K. G., Browning, J. V., Schmelz, W. J., Kopp, R. E., Mountain, G. S., & Wright, J. D. (2020). Cenozoic Sea-level and cryospheric evolution fromdeep-sea geochemical and continental margin records. *Science Advances*, *6*, eaaz1346.

Milliman, J. D., & Farnsworth, K. L. (2011). *River discharge to the Coastal Ocean—A global synthesis* (p. 384). Cambridge University Press.

Mitchum, R. M. (1985). Seismic stratigraphy expression of submarine fans. In Berg, O.R., Wolverton, G.D. (Eds.), *Seismic stratigraphy* (Vol. *39*, pp. 117–138). American Association of Petroleum Geologist Bulletin.

Moscardelli, L., Wood, L., & Mann, P. (2006). Mass-transport complexes and associated processes in the offshore area of Trinidad and Venezuela. *American Association of Petroleum Geologists, Bulletin*, *90*, 1059–1088.

Olariu, C., & Steel, R. J. (2009). Influence of point-source sediment supply on modern shelf-slope morphology: Implications for interpretation of ancient shelf margins. *Basin Research*, *215*, 484–501.

Pellegrini, C., Asioli, A., Bohacs, K. M., Drexler, T. M., Feldman, H. R., Sweet, M. L., Maselli, V., Rovere, M., Gamberi, F., Valle, G. D., & Trincardi, F. (2018). The late Pleistocene Po River lowstand wedge in the Adriatic Sea: Controls on architecture variability and sediment partitioning. *Marine and Petroleum Geology*, *96*, 16–50.

Petter, A. L., & Steel, R. J. (2006). Hyperpycnal flow variability and slope organization on an Eocene shelf margin, Central Basin, Spitsbergen. *American Association of Petroleum Geologists, Bulletin*, *90*(10), 1451–1472.

Posamentier, H. W., & Allen, G. P. (1999). Siliciclastic sequence stratigraphy: Concepts and applications. *SEPM Concepts in Sedimentology and Paleontology*, *7*, 210.

Posamentier, H. W., Jervey, M. T., & Vail, P. R. (1988). Eustatic controls on clastic deposition II—Sequence and systems tractmodels. In C. K. Wilgus, B. S. Hastings, C. G. S. C. Kendall, H. W. Posa-mentier, C. A. Ross, & J. C. van Wagoner (Eds.), *Sea-level change: An integrated approach* (Vol. *42*, pp. 109–124). SEPM Special Publications.

Posamentier, W. H., Kolla, V., & Liu, H. (2019). An overview of deep-water turbidite deposition. *Acta 659 Sedimentologica Sinica*, *37*, 879–903. [In Chinese].

Pratson, L., Swenson, J., Kettner, A., Fedele, J., Postma, G., Niedoroda, A., & Hutton, E. (2004). Modeling continental shelf formation. *Oceanography*, *174*, 118.

Prince, G. D., & Burgess, P. M. (2013). Numerical modeling of falling-stage topset aggradation: implications for distinguishing between forced and unforced regressions in the geological record. *Journal of Sedimentary Research*, *83*, 767–781.

Qi, K., Gong, C., Fauquembergue, K., & Zhou, Y. (2022). Did eustatic sea-level control deep-water systems at Milankovitch and timescale? An answer from Quaternary Pearl River margin. *Sedimentary Geology*, *439*, 106217.

Rich, J. L. (1951). Three critical environments of deposition and criteria for recognition of rocks deposited in each of them. *Geological Society of America Bulletin*, *65*, 1–20.

Ru, K., & Pigott, J. D. (1986). Episodic rifting and subsidence in the South China Sea. *AAPG Bulletin*, *70*(9), 1136–1155.

Steel, R. J., & Olsen, T. (2002). Clinoforms, clinoform trajectories and deepwater sands. In J. M. Armentrout & N. C. Rosen (Eds.), *Sequence-stratigraphic models for exploration and production: Evolving methodology, emerging models and application histories: SEPM, Gulf Coast Section, 22nd Annual Research Conference, Proceedings*, CD-ROM, 367–381.

Syvitski, J. P., & Milliman, J. D. (2007). Geology, geography, and humans battle for dominance over the delivery of fluvial sediment to the coastal ocean. *The Journal of Geology*, *115*(1), 1–19.

Tucker, G. E., & Slingerland, R. L. (1994). Erosional dynamics, flexural isostasy, and long-lived escarpments: A numerical modeling study. *Journal of Geophysical Research-Solid Earth*, *99*, 12229–12243.

Vail, P. R., Mitchum, R. M., & Thompson, S. (1977). Seismic stratigraphy and global changes of sea level, part 4, global cycles of relative changes of sea level. In C. E. Payton (Ed.), *Seismic stratigraphy, application to hydrocarbon exploration* (Vol. *26*, pp. 83–97). American Association of Petroleum Geologists Bulletin.

Van Wagoner, J. C., Mitchum, R. M., Campion, K. M., & Rahmanian, V. D. (1990). Siliciclastic sequence stratigraphy in well logs, cores, and outcrops: Concepts for highresolution correlation of time and facies. *American Association of Petroleum Geologists Bulletin*, *7*, 55.

Wang, G. C., Cao, K., & Zhang, K. X. (2011). Spatio-temperal frame of tectonic uplift stages of the Tibetan plateau in the Cenozoic. *Science China: Earth Sciences*, *54*(1), 29–44.

Wang, X., Wang, Y., He, M., Chen, W., Zhuo, H., Gao, S., Wang, M., & Zhou, J. (2017). Genesis and evolution of the mass transport deposits in the middle segment of the Pearl River canyon, South China Sea: Insights from 3D seismic data. *Marine and Petroleum Geology*, *88*, 555–574.

Wang, X., Wang, Y., Tan, M., & Cai, F. (2020). Deep-water deposition in response to sea-level fluctuations in the past 30 Kyr on the northern margin of the South China Sea. *Deep-Sea Research Part I*, *163*, 103317.

Xie, Z., Sun, L., Pang, X., Zheng, J., & Sun, Z. (2017). Origin of the Dongsha event in the South China Sea. *Marine Geophysical Research*, *38*, 357–371.

Xue, W., Zheng, Z., Zhan, H., & Lei, Y. (1996). *Sea-level environmental changes during the Quaternary in the northern South China Sea* (p. 12). Qingdao Ocean University Press. [in Chinese].

Yao, B. C. (1999). Tectonic characteristics of northwest subbasin and seafloor spreading history of South China Sea in Cenozoic. *Tropic Oceanology*, *18*, 7–15. [in Chinese with English Abstract].

Yao, B. C., & Yang, M. (2008). Tectonic movements in the late Cenozoic and gas hydrate resources in the South China Sea. *Marine Geology & Quaternary Geology*, *28*, 93–100. [in Chinese with English Abstract].

Zhang, J., Kim, W., Olariu, C., & Steel, R. J. (2019). Accommodation-versus supply-dominated systems for sediment partitioning to deep water. *Geology*, *47*, 419–422.

Zhang, J., Steel, R. J., & Ambrose, W. (2017). Paleocene Wilcox cross-shelf channel-belt history and shelf-margin growth: Key to Gulf of Mexico sediment delivery. *Sedimentary Geology*, *362*, 53–65.

Zhang, P., Molnar, P., & Downs, W. R. (2001). Increased sedimentation rates and grain sizes 2 ± 4 Myr ago due to the influence of climate change on erosion rates. *Nature*, *410*(19), 891–897.

Zhao, F., Alves, T. M., Wu, S., Li, W., Huuse, M., Mi, L., Sun, Q., & Ma, B. (2016). Prolonged post-rift magmatism on highly extended crust of divergent continental margins (Baiyun sag, South China Sea). *Earth and Planetary Science Letters*, *445*, 79–91.

Zhao, S. J., Wu, S. G., Shi, H., Dong, D., Chen, R., & Wang, Y. (2012). Structures and dynamic mechanism related to the Donghsa movement at the northern margin of South China Sea. *Progress in Geophysics*, *27*, 1008–1019.

Zhong, D., & Ding, L. (1996). The uplifting process and mechanism of the Qinghai-Tibet plateau. *Science China: Earth Sciences*, *26*(4), 289–295.

Zhuo, H., Wang, Y., Shi, H., He, M., Chen, W., Li, H., Wang, Y., & Yan, W. (2015). Contrasting fluvial styles across the mid-Pleistocene climate transition in the northern shelf of the South China Sea: Evidence from 3D seismic data. *Quaternary Science Reviews*, *129*, 128–146.

SUPPORTING INFORMATION

Additional supporting information can be found online in the Supporting Information section at the end of this article.

How to cite this article: Qi, K., Gong, C., Zhang, J., Andresen, K. J., & Jin, Z. (2022). Relative sea-level control on the building of two distinct shelf-margin clinothems on the late-Quaternary Pearl River margin: Insights from numerical stratigraphic forward modelling. *Basin Research*, *00*, 1–23. https://doi.org/10.1111/bre.12738